3D stratigraphic architecture, sedimentary budget, and sources of the Lower and Middle Triassic strata of western Canada: evidence for a major basin structural reorganization

Vincent Crombez, Sébastien Rohais, François Baudin, Tristan Euzen, John-Paul Zonneveld, Matthew Power

3D stratigraphic architecture, sedimentary budget, and sources of the Lower and Middle Triassic strata of Western Canada: evidence for a major basin structural reorganization

Abbreviated title: Montney-Doig Fms stratigraphic architecture

CROMBEZ Vincent*[1 2#], ROHAIS Sébastien [1], BAUDIN François [2], EUZEN Tristan [3],
ZONNEVELD John-Paul [4], POWER Matthew [5]

1 - IFP Énergies nouvelles, 1 et 4 Avenue de Bois-Préau, 92852 Rueil-Malmaison, France.

2 - Sorbonne Université, CNRS, ISTeP, 4 place Jussieu, 75005 Paris, France.

3 - IFP Technologies (Canada) Inc., Suite 810, 744 - 4th Avenue S.W., Calgary, AB, Canada.

4 – University of Alberta, 116 St and 85 Ave, Edmonton, AB, Canada.

5 – SGS Canada Inc., 3260 Production Way, Burnaby, BC, Canada.

– presently at CSIRO Deep Earth Imaging Future Science Platform, ARRC, 26 Dick Perry Avenue, Kensington, WA 6151

* – Corresponding author, (crombez.v@gmail.com)

ABSTRACT

This study focuses on the Lower-Middle Triassic Montney, Sunset Prairie, Doig, and, Halfway formations from the foreland basin of the Canadian Cordillera (Alberta and British Columbia). Based on core and outcrop descriptions, correlation of 400 wells, and, on mineralogical analyses, this study interprets the basin-scale, 3D-stratigraphic architecture of these formations and discusses the controls on its evolution.

Well correlation highlights four sequences (1-4) interpreted to occur in two second-order cycles (A and B). In this work, the Lower Triassic Montney Formation and the early Middle Triassic Sunset Prairie Formation are interpreted to consist of three third-order sequences (1-3) related to the first second-order cycle (cycle A). The Middle Triassic Doig and Halfway formations are interpreted to consist of a fourth sequence (4) related to a second-order cycle (cycle B). Integration of stratigraphic surfaces with previously published biostratigraphic analyses emphasizes a major time gap of ca. 2 Ma between these two cycles interpreted to record a major reorganization of the basin. Mineralogical analyses suggest that during cycle A, sediments were delivered from the east (Canadian Shield) whereas in cycle B additional sources from the west (proto Canadian Cordillera) occurred. This study shows the stratigraphic architecture evolution was affected by the structural heritage of the basin and continental geodynamic evolution. This study provides a large-scale understanding on the controls of the stratigraphic architecture of Lower and Middle Triassic strata suggesting local and regional controls on the reservoir extension and unconventional plays configuration within these strata.

The geodynamic evolution of the Western Canada Sedimentary Basin (WCSB) was previously divided into two stages: (1) a passive margin prior to the Jurassic and (2) a foreland basin from the mid-Jurassic to the present day (Price, 1994; Monger and Price, 2002). Nonetheless, recent studies on the Triassic strata from the WCSB (Golding *et al.,* 2015 a; Onoué *et al.,* 2016) and on the regional geodynamic evolution of Western Canada (Beranek and Mortensen, 2011; Rohais *et al.,* 2018) present a more complex geodynamic and paleogeographic context during that time interval. However, these previous works did not integrate a detailed 3D stratigraphic architecture of the Lower and Middle Triassic strata into their analysis of the basin evolution.

In the past decade, the development of multi-disciplinary source-to-sink studies guided the analysis of sedimentary basins toward an integrated discipline. This type of study greatly helps in understanding (1) the local and regional evolution of basin sediment sources, and, (2) the structural and geodynamical evolution of the area based on the reading of the sedimentary records. It implies (1) the restoration of sedimentary basin architectures based on sequence stratigraphy to establish sedimentary budgets related to paleogeographic evolution (e.g. Rouby *et al.,* 2009; Guillocheau *et al.,* 2012; Rohais *et al.,* 2016), (2) the determination of sources of sediments through provenance studies (Golding *et al.,* 2015 a, 2016), (3) the restoration of catchments areas and characterization of the eroded material (Grimaud *et al.,* 2018), and, (4) the integration of basin deformation and mechanisms driving subsidence (Contreras *et al.*, 2010; Matenco *et al.,* 2013; Guillocheau *et al.,* 2015). Major advances in the dynamics of sedimentary basins have been proposed in recent years, for example on the Scandinavian (Martinsen *et al.,* 2010), Mediterranean (Leroux *et al.,* 2017) and Atlantic (Baby *et al.,* 2018) margins.

The present work focuses on the Triassic Montney and Doig formations within the WCSB, following a source-to-sink approach. With its huge shale-oil and shale-gas potential and the development of new petroleum prospects in this interval, a new wealth of well data is available. This enables us to present a novel stratigraphic architecture for this interval and discuss the controls on the stratigraphic evolution of an organic-rich interval at basin scale and investigate its controls. This will result in a

better estimation of the extent and geometric configuration of reservoirs within shale-plays in Western Canadian Lower and Middle Triassic successions.

The workflow developed here is divided in three main steps: (1) a study of the 3D stratigraphic architecture of the Lower and Middle Triassic strata based on well-log correlations calibrated with data from core and outcrop data following the concepts developed by Posamentier and Walker (2006) for facies and paleoenvironmental characterisation, and, Catuneanu (2006) for stratigraphic correlations, (2) the integration of this stratigraphic architecture in an existing temporal framework based on previous biostratigraphic studies (Orchard and Zonneveld, 2009; Golding *et al.,* 2015 b; Henderson and Schoepfer, 2017), (3) an analysis of the relationship between the main sequence boundaries and the regional context, and, (4) the study of the sediment mineralogy variation across the interval and its implication on the sediment provenance. This analysis provides insight into the regional and local controls of geodynamics on the paleogeographic evolution and stratigraphic architecture of the Montney, Sunset Prairie, Doig and Halfway formations in the WCSB.

LOWER AND MIDDLE TRIASSIC STRATA: WESTERN CANADA SEDIMENTARY BASIN

In Western Canada, Triassic strata are present in two basins: (1) the Western Canada Sedimentary Basin (WCSB, **Fig. 1**) and (2) the Williston Basin (North Dakota and South Saskatchewan, Edwards *et al.,* 1994). In the Williston basin, the Triassic interval consists of poorly-dated, continental red bed deposits (Cumming, 1956; Carlson, 1968; Edwards *et al.,* 1994, Butcher *et al.,* 2012) whereas in the WCSB, the Lower to Middle Triassic strata preserves a variety of marine and marginal marine environments (Armitage, 1962, Davies, 1997; Davies *et al.,* 1997; Zonneveld *et al*., 1997; Dixon, 2000; Zonneveld *et al.,* 2001; Zonneveld, 2001; Orchard and Zonneveld, 2009, Furlong *et al.,* 2018 a). In the subsurface of the WCSB marine deposits of the Lower and Middle Triassic (approx. 15 Ma of deposition, Orchard and Tozer, 1997) are divided into four formations from older to younger: the Montney, Sunset Prairie, Doig and, Halfway formations.

In the WCSB (**Fig. 1**), Lower and Middle Triassic strata occur stratigraphically between the Permian Belloy Formation and the Upper Triassic Charlie Lake Formation or the regional sub-Jurassic erosional unconformity. The study interval consists primarily of fine-grained sandstone, siltstone, and shale with locally-occurring, sandy, bioclastic packstone and grainstone beds (Armitage, 1962; Gibson, 1974; Gibson, 1975; Davies, 1997; Davies *et al.,* 1997; Zonneveld *et al.,* 1997, 2001, 2010 a, 2010 b; Zonneveld, 2001; Crombez *et al.,* 2016). Studies on the sedimentology and depositional environments of this interval highlight a wave-dominated environment, including phosphatic shale layers (Armitage, 1962, Gibson, 1974; Gibson, 1975; Evoy and Moslow, 1995; Davies *et al.,* 1997; Evoy, 1995, 1997; Zonneveld *et al.,* 1997; 2001; 2010 a, Zonneveld, 2001; Golding *et al.,* 2014; Crombez *et al.,* 2016; Euzen *et al.,* 2018), turbiditic deposits (Moslow and Davies, 1997; Crombez *et al.,* 2016) and evaporitic environments for the top of the Middle Triassic deposits (Davies, 1997; Zonneveld *et al.,* 1997, 2001; Zonneveld, 2000). Various biostratigraphic studies (Orchard and Tozer, 1997; Zonneveld *et al.,* 1997; Orchard and Zonneveld, 2009; Golding *et al.,* 2015 b; Henderson and Schoepfer, 2017; Henderson *et al.,* 2018) show that the Montney Formation was deposited during the Latest Permian and Early Triassic and the Doig and Halfway formations were deposited during the Middle to Late Triassic. The geodynamic setting during deposition of Lower and Middle Triassic strata is still a matter of debate: according to Davies *et al.* (1997), the Montney and Doig formations were deposited on the western passive margin of the Pangaea supercontinent, whereas Ferri and Zonneveld (2008) and Golding *et al.* (2015 a) suggested that these formations were deposited in an early foreland basin based on sediment provenance analyses. More recently, subsidence backstripping has corroborated the early foreland setting hypothesis (Rohais *et al.,* 2018).

In the past, numerous studies have focused on the sub-regional stratigraphic architecture of the Montney (e.g. Markhasin, 1997; Kendall, 1999; Panek, 2000) or Doig formations (Evoy, 1995, 1997; Harris, 2000, Golding *et al.,* 2015 b). More regional and older studies provided a stratigraphic framework for the Montney and Doig formations (Gibson and Barclay, 1989; Embry and Gibson, 1995; Embry, 1997; Davies *et al.,* 1997), but did not benefit from the wealth of new data made

117 available by the recent development of the distal unconventional part of the Montney-Doig play.
118 These studies highlight two second-order cycles: one in the Montney Formation; another one in the
119 Doig and Halfway formations; and several third-order sequences within each second-order cycle.

120 The geometry and the extent of those sequences is one of the main controls on hydrocarbon
121 reservoirs localization in these formations. Redefining a basin-scale stratigraphic architecture (*sensu*
122 Catuneanu, 2006) based on the new wealth of well data available and understanding its link with the
123 continent evolution is paramount for hydrocarbons exploration.

124 ## DATA AND METHODS

125 ### Data

126 The present work is based on data from over 2000 wells, provided by operators to the Alberta Energy
127 Regulator and the British Columbia Oil and Gas Commission and uploaded through data providers
128 including GeowebWorks, IHS Data Manager and Divestco Energisite. Well logs were collected and
129 gathered in a PETREL database. This dataset is completed by 22 sedimentological sections from 18
130 cores and 4 outcrops and cuttings samples through the entire study interval from three wells (**Fig. 1**).
131 From this database, 400 wells were selected along 18 regional cross-sections to reconstruct the
132 stratigraphic architecture of the Lower and Middle Triassic (**Fig. 1**).

133 ### Methods

134 #### *Sedimentology and sequence stratigraphy*

135 Sedimentary facies were identified in core and depositional environments were interpreted.
136 Correlation of core descriptions with available well logs allowed interpretations to be upscaled
137 through the interval of interest facilitating regional sequence stratigraphic correlations (following
138 methods presented in Crombez *et al. (*2016*)*. This interpretation was complemented by description
139 and analysis of outcrop sections of Middle Triassic strata (**Fig. 1**). The analysis of the stacking pattern
140 and spatial distribution of depositional environments makes it possible to define shoreline

trajectories (Helland-Hansen and Martinsen, 1996; Helland-Hansen and Hampson, 2009) and to identify major stratigraphic surfaces: end of regression, end of transgression, onset of base level fall and end of base level fall (Catuneanu, 2006, Catuneanu *et al.,* 2009). Following the terminology proposed by Hunt and Tucker (1992) and Helland-Hansen and Gjelberg (1994), these stratigraphic surfaces were used to reconstruct the 3D stratigraphic architecture of the studied interval. In the present work, the authors aim at providing regional correlation lines across the basin, that can serve as foundations for future works regardless of stratigraphic schools of thoughts. However, the names of the stratigraphic surfaces and the stratigraphic systems tracts refer to a new and local stratigraphic architecture for the Lower and Middle Triassic strata of the WCSB defined by the authors based on Catuneanu *et al.* (2009) perspective on stratigraphy admitting a cyclicity in sedimentary records.

Mineralogical analyses

QEMSCAN analyses (Gottlieb *et al.,* 2000) were performed by SGS Canada Inc. on 201 cuttings samples. QEMSCAN is based on backscattered-electron imaging and energy dispersive X-ray spectroscopy techniques. It identifies individual minerals using a low-count energy-dispersive x-ray database. This system provides a quantification of individual minerals together with an image of their distribution in the samples.

RESULTS

Sedimentary environments and depositional model

Detailed descriptions of the sedimentary facies were presented in previous papers (Crombez *et al.,* 2016; Euzen *et al.,* 2018). In the present study, two additional environments were highlighted: (1) estuarine deposits, and (2) sabkha deposits. **Figure 2** illustrates the different depositional environments with representative core photos and gamma log profiles. In the Lower and Middle Triassic, seven main sedimentary environments are recognized: (1) sabkha environment (**Fig. 2 a**), (2) estuarine and tidal environment (**Fig. 2 b**), (3) foreshore environment (**Fig. 2 c**), (4) shoreface

environment (**Fig. 2 d and e**), (5) turbiditic environment (**Fig. 2 f**), (6) offshore transition environment (**Fig. 2 g**), and, (7) offshore environment (**Fig. 2 h**). The marine depositional environments presented above are characteristic of a wave-dominated shelf (Suter, 2006). In our work, no clear evidence of deltaic environments was highlighted but previous studies identified these environments below the sub-Jurassic unconformity along the erosional edge, especially in the north-eastern part of the basin (e.g. Zonneveld *et al.,* 2010 a, 2010 b; Zonneveld and Moslow, 2018).

Figure 2 illustrates the typical gamma ray profiles of the main environments encountered in this study. The figure shows that tidal deposits present a blocky pattern that is interpreted to represent the sharp transition between heterolithic tidal flat successions with sandy tidal channel units. Shoreface and foreshore deposits present the same coarsening upward trend but with depressed gamma ray profiles interpreted to be linked to the higher sand content. Turbiditic deposits are characterized by a major drop in the gamma radiation interpreted to represent a sharp depositional contact of sandstone above more highly radioactive offshore units. Unlike shoreface and foreshore environments, turbiditic deposits often present fining upward trends, interpreted to represent the lateral migration and/or waning of the turbiditic system. Turbiditic deposits also typically show high amplitude GR variations associated with high frequency changes in depositional energy and, concomitantly, lithology. Lastly, offshore and offshore transition successions present high gamma ray profiles with coarsening upward trends. The recognition of these distinctive patterns provides a means with which to interpret depositional environments and therefore vertical changes in relative depositional bathymetry on well logs (Crombez *et al.,* 2016). However, it is important to note that as the facies recognition is mainly based on well-log pattern some intervals might be misinterpreted, however we are confident on the regional trends highlighted. Here, the absolute value of the gamma ray readings may vary depending on the tools used and the vintage of the data.

Stratigraphic architecture along the 2D well sections

Regional stratigraphic sections

191 The synthetic stratigraphic architecture of the Montney, Sunset Prairie, Doig, and Halfway formations
192 is presented in **figure 3**. On this figure, four sequence boundaries (named after the sequence they
193 form part of) are presented. They delimit four stratigraphic sequences: the first three sequences
194 (sequences 1 -3) within the Montney Formation and the last sequence (sequence 4), within the Doig
195 and Halfway formations. The sequences 1-3 are interpreted to be part of the older second-order
196 cycle (cycle A) described in previous studies (Gibson and Barclay, 1989; Edwards *et al.,* 1994; Davies,
197 1997) and sequence 4 is interpreted to be part of the younger, second-order cycle (cycle B) discussed
198 in the same papers.

199 Three of the eighteen cross sections realized for the present study are presented in this paper (**Figs.**
200 **1; 4-6**). **Figure 4** presents a 375 km long SE-NW section with 25 wells, **figure 5** presents a 275 km long
201 NE-SW section with 18 wells, and **figure 6** presents a 625 km long SSE-NNW with 25 wells. All
202 sections cross the entire lateral extent of Lower and Middle Triassic strata of the subsurface of the
203 WCSB. Along these sections, the study interval lay stratigraphically above the Permian Belloy
204 Formation. In the eastern part of the basin, the studied interval is truncated either by the
205 unconformable Jurassic Gordondale Formation or by the Upper Triassic Coplin unconformity,
206 whereas in the western part, it is capped by the late Middle to Upper Triassic (late Ladinian to
207 Carnian) Charlie Lake Formation. In the present study, all sections are flattened on sequence
208 boundary 4 (SB4).

209 The stratigraphic architecture illustrated on these cross-sections suggests that sequences 1, 2 and 3
210 were only sourced from the east and south, whereas sequence 4 includes sediment sourced from the
211 west and/or south-west. On all well sections: 1) sequence 1 is almost completely preserved except in
212 eastern-most regions; 2) the proximal parts of sequence 2 are missing due to the sub-Jurassic, SB4,
213 and SB3 erosional unconformities; 3) sequence 3 is preserved solely in the deepest part of the basin
214 where it only presents distal deposits below an erosional truncation; and 4) sequence 4 is well
215 preserved in the western part of the basin.

On all sections, it appears that the maximum flooding surface of sequence 2 (MFS2) resulted from a stronger backstep of the shoreline than the MFS of sequence 1 (MFS1), as only the distal part of the transgressive systems tract (TST2) is preserved. Above MFS2, it appears that the basin experienced a major regression trend up to SB4. In cycle A (Montney and Sunset Prairie formations), the second-order MFS is, therefore, interpreted to be MFS2. As cycle B is only composed of sequence 4, the maximum backstep of the sedimentary system is, therefore, recorded during MFS4.

Groundbirch area facies section

Figure 7 provides a detailed correlation of the TST4 and HST4 succession (upper part of the study interval) from the Groundbirch area in British Columbia. Well log signatures were interpreted based on sedimentological descriptions of core from the subsurface of Alberta and outcrop from the Williston Lake area. **Figure 7** shows that TST4 (parasequence 1) gets thinner toward the centre of the well section. In the regressive part of sequence 4, marine deposits identified from well logs are highlighted on this figure (in sedimentary parasequences 2 to 5, thinning from the west to the east). In addition to this thickening toward the east, no fluviatile deposits were identified in the Middle Triassic (Doig and Halfway formations) interval.

3D stratigraphic evolution

Cycle A

Figures 4-6 illustrate the stratigraphic evolution along three 2D profiles. **Figure 8** shows the distribution of sedimentary deposits during the third-order systems tracts of cycle A (Montney and Sunset Prairie formations).

The maximum thickness of TST1 (up to 80 m) occurs along the eastern part of the basin (**Fig. 8 a**) where it is primarily composed of foreshore to shoreface deposits. The maximum thickness of HST1 (**Fig. 8 b**), is located in the northern part of the basin, where thicknesses can locally reach up to 120 m. The falling stage systems tract 1 (FSST1) (**Fig. 8 c**) is poorly developed and only preserved in the central part of the basin where it consists of massive turbiditic deposits (Crombez *et al.,* 2016).

241 The lowstand deposits of sequence 2 are preserved primarily in the central part of the basin (**Fig. 8 d**)
242 where fine-grained turbidites occur interbedded with offshore deposits (up to 90 m). The North-
243 South depositional fairway, extending from the cordillera in the South to the LST2 depocentre in the
244 North, consists mainly of turbiditic channel and overbank deposits. This suggests that during this
245 lowstand period, a large part of the sedimentary input may have come from the South. In this
246 interval the turbidites are often associated with HCS and are, therefore, interpreted as shelf
247 turbidites. TST2 consists of starved deposits in the basin (**Fig. 8 e**). In our interpretation, based on
248 sequence stratigraphic principles, the area of maximum thickness was likely located a few kilometres
249 beyond the sub-Jurassic erosion edge to the east. HST2 records a significant progradation of the
250 sedimentary system (**Fig. 8 f**), from shoreface in the east to offshore toward the west. However, the
251 maximum thickness is still located in the southern and eastern parts of the basin and can reach up to
252 100 m. Above HST2, the FSST2 is poorly preserved due to erosion by SB3 and SB4. In the basin, it can
253 locally reach 40 m in thickness (**Fig. 8 g**).

254 **Fig. 8 (h-k)** presents the thickness of sequence 3. In this figure, it appears that most of the preserved
255 part of sequence 3 occurs below the SB4 level of erosion. The maximum thickness of LST3 (**Fig. 8 h**) is
256 located in the western part of the basin, along the deformation limit. Shoreface and offshore
257 deposits can reach thicknesses of up to 100 m. In the present-day configuration, TST3 only presents,
258 offshore to offshore transition, starved sedimentation and is only preserved in the west-central part
259 of the basin (**Fig. 8 i**). Both HST3 and FSST3 (**Figs. 8 j and k**) are also only preserved in the western
260 part of the basin, where mainly offshore to offshore transition deposits can reach thicknesses up to
261 70 m.

262 **Figure 9 a** presents isopach maps of the three third-order sequences within cycle A (Montney
263 Formation). It shows that these three sequences do not have the same areas of maximum sediment
264 accumulation. During sequence 1, maximum accumulation occurred in the northern part and eastern
265 margin of the basin. During sequence 2, the maximum accumulation shifted to the central part of the
266 basin. In sequence 3, the depocentre of the preserved parts of the sedimentary succession is located

in the western part of the basin. **Fig. 9 a** also illustrates the location of the main structural elements below the Triassic strata: the Hay River shear zone (HRSZ) and the inherited structure from the Palaeozoic Peace River Arch (PRA) collapse (The Leduc reef indicates the margin of the PRA, O'Connell, 1994; Switzer *et al.,* 1994; Wright *et al.,* 1994). On **figure 9,** it is apparent that the maximum thickness of sequence 1 occurs north of the HRSZ, while the maximum thickness of sequence 2 was deposited in the basin centre above the former PRA. **Figure 9** shows that the preserved parts of sequence 3 are also located above the PRA. Based on the upscaling of the sedimentary facies into three broad depositional environments, **Figure 9 b** presents schematic paleogeographic maps of cycle A. The maps each represent a snapshot of the paleogeography at the end of the lowstand of each third-order sequence. Black arrows illustrate dominant sedimentary inputs from the north-east, the east and the south-east during deposition of cycle A (**Fig. 9 b**). These maps are built using the isopachs of the last systems tracts of each sequence. This assumes that the decrease of the sedimentary thickness coincides with the slope. It is therefore important to keep in mind when interpreting these maps that due to the spacing between the correlation lines, the maps only present a global view of the paleogeography and are unlikely to capture the high-resolution heterogeneities in the sedimentary system. In addition, as tidal and shoreface environments are laterally equivalent and their relative distribution in mainly controlled by the basin physiography and the wave activity, and are poorly preserved in this case study, they are gathered and presented as shallow deposits on these maps.

Cycle B

LST4 is not preserved in the subsurface of the WCSB (**Fig. 10 a**). **Figure 10 a** shows that the TST4 maximum thickness occurs in a halo shape with a maximum thickness of up to 40 m. This figure also shows that during HST4 the maximum thickness is recorded along the present-day deformation limit in the western part of the basin, where the thickness can reach up to 225 m. More proximal facies, and the thickening of this cycle near the deformation limit, suggests that sedimentary input was

likely from the west as well as the east. Finally, evidence of large-scale structural controls on depositional thickness are not observed (**Fig. 10 a**).

Reconstruction of the stratigraphic architecture of the Montney, Sunset Prairie, Doig, and Halfway formations show that cycle A (Montney and Sunset Prairie formations) and cycle B (Doig and Halfway formations) are separated by a major erosional unconformity (also described by Golding *et al.,* 2014; Furlong *et al.,* 2018 a, b). In cycle A, the basin shows a progradation of the sedimentary system (observed from the evolution of the systems tracts depocentres) during the time interval between MFS2 and SB4. At the end of sequence 3, it appears that the basin experienced major subaerial exposure. **Figure 10 b** suggests a completely different paleogeography in cycle B compared to cycle A. Our interpretation suggests that during this cycle, the WCSB experienced sedimentary input from both the continent to the east as well as from a western source. Indeed, stratigraphic thicknesses and sedimentary facies (**Fig. 7**) suggest that sedimentary inputs during TST4 came from both the east and the west whereas during HST4 they may have been sourced primarily from the west (**Fig. 7**). Above SB4, stratigraphic correlations suggest that the basin was becoming increasingly restricted culminating in deposition of sabkha environments in the Charlie Lake Formation (**Fig. 4-7**).

Mineralogy

The results of the QEMSCAN analyses are presented in **figure 11**. On this figure, sequences are represented by different colours and symbols correspond to different wells which are representative of proximal and distal areas of the basin. **Figure 11 a** shows that in the study interval clay content is low (average of 14 wt. %) but can reach up to 35 wt. %. Quartz, feldspar, and mica (Q-F-M) are the dominant minerals (from 25 wt. % to 80 wt. % with an average of 55 wt. %), carbonates represent 27 wt. % on average (from 10 wt. % to 70 wt. %) (**Fig. 11 a**). Cycle B (Doig and Halfway formations; average Q-F-M = 52 wt. %, clay = 8 wt. % and carbonate = 40 wt. %) has less clay and more carbonate than cycle A (Montney and Sunset Prairie formations; Q-F-M = 58 wt. %, clay = 17 wt. %; quartz

316 versus carbonate = 25 wt. %) (**Fig. 11 a**). These QEMSCAN analyses show the occurrence of distinct
317 mineral trends in cycles A and B.

318 **DISCUSSION**

319 **Stratigraphic record, eustatic variations and regional geodynamic evolution**

320 In the present study, we highlight 4 stratigraphic sequences (**Fig. 3**). Three occur in the Montney
321 Formation (sequences 1-3) and one in the Doig and Halfway formations (sequence 4). Previous
322 studies on biostratigraphy (Orchard and Tozer, 1997; Orchard and Zonneveld, 2009; Golding *et al.,*
323 2014, Golding *et al.,* 2015 b; Henderson and Schoepfer, 2017; Henderson *et al.,* 2018) provide a
324 chronostratigraphic framework for these sequences. In the present work we chose to use 250.0 Ma
325 as the date of the boundary between the Induan and the Olenekian as suggested by Henderson *et al.*
326 *(*2018). Based on the biostratigraphic data of these studies, the three sequences that were identified
327 in the Montney and the recently defined Sunset Prairie formations are interpreted to have been
328 deposited primarily during the Lower Triassic and the earliest Middle Triassic whereas the sequence
329 encompassing the Doig, and Halfway formations (cycle B) were deposited primarily during the Middle
330 Triassic.

331 To better calibrate the ages of the third-order sequences within the Montney Formation, **Figure 12 a**
332 presents the high-frequency, global eustatic sea-level variations (Hardenbol *et al.,* 1998). On **Figure**
333 **12 a**, this global curve presents three rise and fall cycles in the Lower Triassic and three in the Middle
334 Triassic. In the present work, as no major basin scale hiatus was highlighted between sequence 1, 2
335 and 3 it is assumed that three high sea levels within the Lower Triassic present on **Figure 12 a** were
336 approximately recorded in the stratigraphy by MFS1, 2 and 3 of our stratigraphic architecture (**fig. 12**
337 **b**). According to our interpretation of the stratigraphic architecture (**fig. 12 c**), sequence 2 and 3
338 represent respectively the HST and FSST of a second-order cycle A and major erosional surface SB4
339 corresponds to the subaerial sequence boundary underneath the second-order cycle B. Recent work
340 on the Doig Phosphate Zone (Golding *et al.,* 2015 b) concluded that deposition of this interval was

diachronous, with early Anisian deposits in the west and middle Anisian deposits to the east of their study area. Stratigraphic correlation of the present study suggests that they are part of the same stratigraphic interval deposited across the late early Anisian to the middle Anisian. On **figure 12 c**, TST4 is interpreted to be linked to the long rise of sea level that is present in the late early to middle Anisian. As the last eustatic cycle recorded in cycle A ended in the earliest Anisian, the association of the high amplitude eustatic rise from the middle Anisian with the TST4 implies that a large part of the early Anisian eustatic cycle present on the curve was not recorded in the basin. In the present work, this unrecorded cycle (**fig. 12 b**) is interpreted to be the expression of the second-order LST of cycle B at the boundary between the Montney and Doig formations (**fig. 12 c**). This is supported by the fact that in the Williston lake area, a major unconformity incises down to sequence 2 and by the fact that in the WCSB, remnants of early Anisian marine sediments are preserved below the Doig Formation in the Sunset Prairie Formation, as discussed in Furlong *et al*. (2018 a and b). As TST4 (**fig. 12 c**) is interpreted as a second-order transgression, the Doig Phosphate Zone may have been deposited from the late early Anisian through the early upper Anisian. As one third order eustatic cycle is missing in the early Anisian, we suggest that a hiatus and a major erosion occurred at this time and that only a small fraction of early Anisian deposits are present in the preserved part of the basin. Above MFS4, the eustatic curve shows two episodes of relative sea level fall (**Fig. 12 a**). As in cycle A, the regression of the Middle Triassic cycle may consist of several third-order sequences. In the Anisian and Ladinian, no major cycle boundary was highlighted at basin-scale, but the two eustatic cycles may correspond to the two prograding cycles present in the Williston Lake area and elsewhere as reported in previous studies (Embry and Gibson, 1995; Davies *et al.,* 1997; Embry, 1997, Gibson and Barclay, 1989).

Figure 12, summarizes our sequence stratigraphic interpretation of the Lower and Middle Triassic in western Canada. It shows that the global eustatic sea-level variations (**Fig. 12 a**, from Hardenbol *et al.,* 1998) do not perfectly fit with our regional stratigraphic observations and interpretations from our study (**fig. 12 b, c**): (1) the highest sea level of cycle A does not coincide with MFS2 (interpreted

as the second order MFS of this cycle), (2) the unrecorded cycle does not correspond to a major drop of sea level, (3) cycle B shows two high-amplitude rises of the sea level. Misfit between the stratigraphic architecture of a basin and the depositional sequence described on the world eustatic curves has been observed by previous research in various case studies (e.g. Miall, 1986, 2009). As the Montney, Sunset Prairie, Doig, and Halfway formations consist primarily of marine deposits, relative variations of sea level registered in the sedimentary records result from global eustatic variations combined with regional tectonism impact. The misfit between the global eustatic variations and our stratigraphic framework suggests the strong influence of regional tectonics (e.g. regional uplift) on relative sea-level variations during the deposition of the Lower and Middle Triassic Strata. In order to investigate this structural control, we compute a composite relative eustatic curve fitting our interpretation, by adding two trends (a medium-term curve, with a period of 5.5 Ma and an amplitude of ca. 35 m and a long-term curve, with an amplitude of ca. 25 m, **Fig. 12 d**) to the eustatic curves of Hardenbol *et al.* (1998). The periods and the amplitudes of these two curves were adjusted, in order to match the trends of the composite curve with the regional stratigraphic observations. As the basin underwent complex structural evolution (Rohais *et al.,* 2018), those curves are interpreted to represent the impact of a small, continuous, continental uplift (long-term curve) and the footprint of regional geodynamics resulting in more punctual and transient structural regional uplift and subsidence (medium-term curve) on relative sea-level (Haq *et al.,* 1987). On **Fig. 12 d**, it appears that the major lowstand conditions between cycle A and cycle B coincides with a minimum in the medium-term curve. This suggests that this sequence boundary was partly controlled by regional tectonic activity, likely the motion of western terranes (Beranek and Mortensen, 2011; Golding *et al.,* 2015 a).

The integration of the stratigraphic architecture in global and regional eustatic variations supports that the geodynamic evolution of the study area and the related structural evolution of the basin largely affected relative sea level and, therefore, partially controlled the stratigraphic architecture of Lower and Middle Triassic strata in the subsurface of the WCSB.

Sediment sources and inputs

The integration of the stratigraphic architecture in a chronostratigraphic framework shows that the three sequences (1-3) of the Montney and Sunset Prairie formations (cycle A) were deposited over approximately 5 Ma whereas the single Middle Triassic cycle (cycle B) was deposited over more than 8 Ma. Isopach maps were used to compute the volume of sediment preserved in cycles A and B. In cycle A, 44,000 km^3 of sediments occur in the subsurface of Alberta and British Columbia whereas in cycle B, 10,000 km^3 are present. These volumes do not include any estimation of the parts that were eroded by the Jurassic (from cycles A and B) or the second-order cycle boundary between cycles A and B (from cycle A). Estimated average sediment fluxes in cycles A and B were computed based on preserved sediment volumes and cycle duration. It shows a major drop at the boundary between cycle A and cycle B (from 12,000 km^3/Ma to 1,600 km^3/Ma in cycle B, including a 30% increase of the volume to account for initial porosity and assuming no carbonate production). In detail, sequences 1-3 (cycle A) exhibits minimal variation in sediment flux (respectively 11,000, 18,000, and 7,900 km^3/Ma) considering that the top of sequence 3 was affected by the erosion of the SB4. Although **figures 4-6** show that sub-Jurassic erosion is a major control on the preserved volumes of sediments, a drastic drop (one order of magnitude) of the sediment supply is likely to have happened at the cycle A – B boundary (from 12,000 to 1,600 km^3/Ma). Indeed, even if we consider that sub-Jurassic erosion removed half of cycle B, the average sedimentation rate of the cycle B (Doig Formation) would still be less than half the sedimentation rate of cycle A (Montney and Sunset Prairie formations).

During the Lower and Middle Triassic, the basin vas located approximately 30°N. According to previous work on paleoclimates and atmospheric circulation on this interval, no climatic shifts are recorded as well as no seasonal influence (Hallam, 1985; Golonka *et al.,* 1994; Davies, 1997 a; Davies et al., 1997; Sellwood and Valdes, 2006; Crombez *et al*., 2017 a), suggesting that the drop of sediment supply between cycles A and B is unlikely to be related to changes in the vegetation cover or increased runoff. Instead, we suggest this change in sedimentation rate is related to modifications

of the continental scale physiography resulting in a decrease of the basin drainage area (Dai and Trenberth, 2002; Milliman and Meade, 1983).

The depocentre evolution for the different systems tracts from cycle A together with the paleoenvironmental reconstruction show that the major part of the sediment input comes from the Canadian Shield (**Fig. 9**) which is consistent with previous stratigraphic evidence (Crombez *et al.,* 2016; Euzen *et al.,* 2018) that emphasized the progradation of the sedimentary system from east to west and also consistent with the occurrence of abundant ephemeral (Zonneveld *et al.,* 2010) and rare perennial (Zonneveld and Moslow, 2014; 2018) deltas on the eastern margin of the basin during deposition of the Montney and Sunset Prairie formations (cycle A). In the Doig and Halfway formations, evidence presented in Golding *et al.* (2015 a) and Harris (2000) suggests sediment input from the west. In the present work, the 3D stratigraphic architecture of cycle B supports the occurrence of sedimentary sources from the west during the Middle Triassic (**Figs. 7 and 10**). Supporting this hypothesis, recent work (Playter *et al.,* 2018; Morris *et al.* 2018) indicates that volcanic arc granite (VAG) or syn-collisional arc granite (SAG) contributed to the Lower and Middle Triassic sediment source including cratonic sources (e.g. the North American Craton). The integration of their observations in recent work on the geodynamic settings on the basin in the Triassic (Rohais *et al.,* 2018) suggests potential sources to the west. Indeed Rohais *et al.* (2018) emphasize a complex stacking of terranes to the west that are potential host for VAG or SAG.

Figure 7 shows thinning of proximal-marine deposits towards the east. This would be consistent with western-sourced sediment if continental successions (e.g. delta plain, flood plain, fluviatile) were present on the eastern edge of cycle B (Doig and Halfway formations). However, such facies were not encountered in core or outcrops either in this or previous studies. The thinning of marine units towards the east is therefore more compatible with sediment sourced from the west. Here, it is important to note that **figure 7** indicates sources from the west but eastern sources are also likely to be present during the deposition of cycle B (Halfway and Doig formations).

444 Analyses of the stratigraphic architecture of cycles A and B emphasize a change of sedimentary
445 sources between the Lower and Middle Triassic. It suggests a major reorganization of the regional
446 paleogeography between the Montney and the Doig formations, during a time interval
447 corresponding to LST4. This turnover is also highlighted by the mineralogy: cycle B contains more
448 detrital carbonate than cycle A, which is consistent with a change of sediment sources (**Fig. 11**).
449 Detailed analysis of the QEMSCAN results shows that the increase in carbonate content is mainly
450 controlled by the increased in dolomite (from 16 wt% in sequence 3 to 30 wt% in sequence 4) rather
451 than by a variation in the calcite content (8 wt% in sequence 3 to 6 wt% in sequence 4). As Palaeozoic
452 formations in Western Canada consist dominantly of carbonates (Price et *al.,* 1972), the areas
453 supplying lithic elements (Quartz, Feldspars and Micas) in Lower and Middle Triassic were most likely
454 reaching the Canadian Shield (Burwarsh *et al.,* 1994; Kent, 1994). Moreover, the occurrence of an
455 increased proportion of detrital carbonates in cycle B (as suggested by Vaisblat *et al.,* 2017 in cycle A)
456 suggests a close proximity to the source as carbonates tend to be rapidly dissolved when eroded.
457 These observations support the interpretation of a major change in basin physiography and in the
458 size of the fluvial catchment area. This resulted in increased reworking of carbonate-dominated
459 Palaeozoic formations to the east with an overall reduction in sediment input from the Canadian
460 Shield associated with increasing sediment supply from newly elevated Palaeozoic formations to the
461 west.

462 The variations of the sediment type and source are not compatible with a passive margin basin
463 setting as suggested by Edwards *et al.* (1994) and Davies *et al.* (1997). The present study supports the
464 interpretation (i.e. Ferri and Zonneveld, 2008; Rohais *et al.,* 2018) that Middle Triassic formations
465 were deposited in a basin that included western sedimentary sources. Based on detrital zircons,
466 Golding *et al.* (2015 a) also suggested the occurrence of western sources and the deposition of the
467 Middle Triassic in an "early foreland basin" or, at least, in a basin where a structural arc is rising
468 towards the west. Further, investigations of regional subsidence rates are presented in Rohais *et al.,*
469 (2018) and agree with this conclusion.

Depocentres and structural settings

For each sequence, the large-scale tectonic control on sedimentation can be assessed through the spatial relationship between the major structural elements of the basin and the thickness distribution.

The HRSZ is reported to have been active during the Precambrian (Hoffman, 1987; Wright *et al.,* 1994) and to have had minimal impact on Triassic strata (Sturrock and Dawson, 1990). Zonneveld and Moslow (2014) discussed the importance of the HRSZ in controlling perennial fluvial systems to the coastline (also discussed in Zonneveld and Moslow, 2018). As discussed herein, the location of the sequence 1 maximum thickness supports the hypothesis that the HRSZ increased local subsidence and thus influenced deposition of the Lowermost Triassic.

Numerous studies have focused on the relative movements of the PRA (Cant, 1988; Barclay *et al.,* 1990; McMechan 1990; O'Connell *et al.,* 1990; Ross, 1990; Eaton *et al.,* 1999), and agreed that the PRA rose during the Precambrian and then started to collapse during the Carboniferous. Other studies have suggested that the Peace River embayment affected the depositon of the Uppermost Triassic deposits (Barclay *et al.,* 1990; Gibson and Barclay, 1989; Davies *et al.,* 1997; Moslow and Davies, 1997; Zonneveld and Moslow, 2014, 2018). In the present work, the maximum thickness of sequence 2 that occurs above the former PRA may suggest the occurrence of bathymetric heritage from the arch collapse. Here, three scenarios are possible: (1) a bathymetric low induced by subsidence of the Dawson Creek Graben Complex; however, even if the LST2 maximum thickness is located above this structure, sequence 1 does not show any thickening in this area, (2) an irregular bathymetry induced by differential compaction of the underlying formations and (3) variation of the subsiding area between sequences 1 and 2: the North of the basin (above the HRSZ) subsided during sequence 1 and the centre of the basin (above the former PRA) subsided during sequence 2 (Moslow and Zaitlin, 2008). Furthermore, detailed studies on systems tract thickness and evolution are needed in this area in order to differentiate between these options.

Finally, it is apparent in **figures 8 (h-k)**, that the preserved part of sequence 3 is located above the PRA. The present work suggests that SB4 was induced by a regional uplift as no major lowstand conditions are described in the global eustatic variations (**fig. 12 a**). Preservation of sequence 3 above the PRA is thus interpreted to be related to reactivation of the ancient structures of the Dawson Creek Graben Complex during the uplift. This reactivation created differential subsidence that increased the preservation of sequence 3 within the Dawson Creek Graben Complex.

The integration of the structural framework of the area with the location of the main depocentres emphasizes that the structural setting during the deposition of the Lower and Middle Triassic strata in the WCSB was not quiescent and that the stratigraphic architecture is affected by pre-existing structures.

Stratigraphic architecture of the Lower and Middle Triassic marine strata of western Canada

Integrating our stratigraphic observations and interpretations in a biostratigraphic and eustatic framework allows to suggest large-scale structural controls on the Lower and Middle Triassic strata of the western Canada sedimentary basin. In addition, it enable us to update the chronostratigraphic chart of this interval (**fig. 12 g**). It is important to note that the part of this figure under the hatched area is conceptual and based on the integration of this work with the world eustatic curves. **Figure 12 g** shows that (1) the Montney and Sunset Prairie formations and (2) the Doig and Halfway formations are two different second-order cycles separated by a major time gap (ca. 2 Ma) associated with both emersion and a major erosion event. In the Montney and Sunset Prairie formations, previous studies have suggested the occurrence of three sequences with a unique regressive trend (Embry and Gibson, 1995; Davies *et al.,* 1997; Embry, 1997, Gibson and Barclay, 1989). In the present study, the Montney Formation appears to be a perfect example of third-order sequence imbrication in a second-order cycle where the terminology of Catuneanu et *al.* (2009) can be applied. The correlation of over 400 wells throughout the basin shows that the maximum flooding surface of the Montney

and Sunset Prairie formations (cycle A) occurred in the second third-order sequence described. In sequence 1, TST1 occurred during a long and smooth rise of sea level resulting in the deposition of backstepping shoreface units (the G-sand of Panek, 2000). In sequence 2, a thick turbiditic interval was deposited during a lowstand in regional sea level (**Fig. 12**). Above SB4, the present work emphasizes the occurrence of estuarine successions (as previous suggested by Zonneveld *et al.,* 2010 a, 2010 b and Zonneveld and Moslow, 2018 in the eastern part of the basin) that were deposited in incised valleys during LST4 (as observed on the Brown Hill outcrop, **Fig. 1**). Above SB4, the basin was influenced by sediment sources from both the east and the west. In the present study, the two distinct prograding cycles of the Middle Triassic are only highlighted in the Williston Lake outcrop and are not described in the basin due to the lack of detail in HST4. However, they are described in previous studies (Embry and Gibson, 1995; Davies *et al.,* 1997; Embry, 1997, Gibson and Barclay, 1989) and, therefore, presented in **figure 12**.

CONCLUSIONS AND PERSPECTIVES

The 3D basin-scale stratigraphic architecture of Lower and Middle Triassic strata in the WCSB was reconstructed based on an extensive network of regional cross-sections and on previous studies. Regional surfaces across Alberta and British Columbia were defined and discussed with regard to the structural and geodynamical evolution of the continent. The key outcomes of this reconstruction are summarized here below:

- Lower and Middle Triassic strata in the WCSB are divided into two second-order cycles (A and B) that are separated by a major erosional surface.
- The limit between the two cycles records a major time gap. This approximately 2 Ma long subaerial exposure is interpreted to be linked to a regional uplift that was probably induced by the initiation of western terrane collisions.
- The first second-order cycle (Montney Formation) was sourced primarily from eastern, continent/craton sources, whereas the second one (Doig and Halfway formations) includes

sedimentary inputs from both the continent and recently elevated western terranes. This turnover is associated with a major change in paleogeographic setting between cycle A and cycle B.

- Deposition of Lower and Middle Triassic strata took place in a tectonically active basin. Observations and interpretations include: (1) the occurrence of regional uplifts, (2) significant sediment thickness changes across the HRSZ, (3) preservation of sequence 3 above the PRA, (4) changes in the paleogeography that induced changes in sedimentary sources.

- A major reorganization of the basin happened between the Lower and Middle Triassic due to the evolution of western terranes.

Lower and Middle Triassic strata of western Canada were, therefore, deposited upon a complex structural framework that influenced the regional evolution of this sedimentary system. It is likely this control will also affect the distribution of sedimentary heterogeneities in this interval, impacting the exploration for both conventional and unconventional in this interval. Further studies on the high-resolution architecture (e.g. Euzen *et al.,* 2018) and stratigraphic modelling (e.g. Crombez *et al.,* 2017 b) of these formations are still required to further understand how this control affect the high-resolution facies distribution within the defined sequences. In addition, 3D advance petroleum system modelling (e.g. Ducros *et al.,* 2017) is still required to fully integrate this high-resolution facies distribution and assess the unconventional potential of the Montney and Doig formations.

ACKNOWLEDGEMENTS

Acknowledgments go to all those who have contributed to this project: IFP Technologies (Canada) Inc., SGS Canada, the Alberta Energy regulator, the BC Oil and Gas Commission, the Geological Survey of Canada, to Schlumberger that provided Petrel academic licenses, and to CSIRO for supporting the corresponding author through writing and publication of this manuscript. L. Schoneveld and D. Dewhurst are also acknowledged for their diligent proofreading of this manuscript.

FIGURE CAPTIONS

Fig. 1. (a) Location of the study area and of the data available for this study (geological map from Reed *et al*., 2005, Triassic subcrop edges from Edwards *et al*., 1994; basin limits from Wright *et al*., 1994). (b) Chronostratigraphic chart of the Lower and Middle Triassic of the Western Canada Sedimentary Basin (Orchard and Zonneveld, 2009; Furlong *et al.,* 2018 a b)

Fig. 2. Facies, major sedimentary environments, and their Gamma Ray patterns (modified from Crombez *et al.,* 2016). (**a**) Reddish heterolithic siltstones and clays with anhydrite nodules, (**b**) wavy- to flaser-bedded, heterolithic siltstones and sandstones with bidirectional current ripples, (**c**) bioclastic sandstones, (**d**) medium-grained sandstone, (**e**) wavy-bedded (concave), heterolithic siltstones and sandstone, (**f**) heterolithic siltstones and sandstones with climbing ripples, (**g**) wavy-bedded (convex), heterolithic siltstones and sandstones, and, (**h**) massive dark grey siltstones.

Fig. 3. Synthetic stratigraphic framework of the Lower and Middle Triassic formation. Four depositional sequences with their internal surfaces are highlighted with different colours. Note that reaching this vertical resolution is only possible using well data, onshore seismic data do not present such details. SP: Sunset Prairie Formation.

Fig. 4. SE-NW well section with stratigraphic correlations. Note that the average distance between wells is ca. 15 km. Supplementary wells were added to the correlation to reduce the spacing in area where correlations were uncertain. On this figure, Gamma-ray log is coloured so that the low

587 radioactive intervals appear in yellow and the highly radioactive intervals appear in dark grey.
588 Location on **figure 1**.

589 **Fig. 5.** NE-SW well section with stratigraphic correlations. Note that the average distance between
590 wells is ca. 15 km. Supplementary wells were added to the correlation to reduce the spacing in area
591 where correlations were uncertain. On this figure, Gamma-ray log is coloured so that the low
592 radioactive intervals appear in yellow and the highly radioactive intervals appear in dark grey.
593 Location on **figure 1**.

594 **Fig. 6.** SSE-NNW well section with stratigraphic correlations. Note that the average distance between
595 wells is ca. 25 km. Supplementary wells were added to the correlation to reduce the spacing in area
596 where correlations were uncertain. On this figure, Gamma-ray log is coloured so that the low
597 radioactive intervals appear in yellow and the highly radioactive intervals appear in dark grey.
598 Location on **figure 1**.

599 **Fig. 7.** Stratigraphic architecture and facies distribution in cycle B over the Groundbirch area. Note
600 this section is 94 km long and has a well spacing <9 km. The cross section suggests western sediment
601 sources during cycle B with a distal pinch-out of the marine deposits toward the east, combined with
602 an eastward progradation. Detailed stratigraphic correlation shows a migration of the basin centre
603 toward the east between TST4 and HST-FSST4. Location on **figure 1**. CL: Charlie Lake Formation.

604 **Fig. 8.** Thickness evolution for each identified systems tract within sequences 1, 2, and 3 (50 m iso-
605 contours). On this figure, the Leduc Reef trend highlights the extent of the former PRA and,
606 therefore, the limit of the Palaeozoic Dawson Creek Graben Complex. This figure highlights the links
607 between the depocentres and the inherited structural elements.

608 **Fig. 9.** (**a**) Thickness evolution in each systems tract in cycle A; (**b**) Paleogeographic maps of cycle A.
609 (structural elements from Berger *et al*., 2008 and Leduc trend from Switzer *et al*., 1994). On this
610 figure "shallow marine to continental" areas gather shorefaces, tidal and non-marine environments.
611 Note that the sedimentary inputs come from the continent to the east.

Fig. 10. (**a**) Thickness evolution in each systems tract in cycle B; (**b**) Paleogeographic maps of cycle B. (structural elements from Berger *et al*., 2008 and Leduc trend from Switzer *et al*., 1994). On this figure, "shallow marine" areas gather shorefaces and tidal environments. Note that no preserved deposits are presented for LST4, it is interpreted to be a major erosion period across the basin at the boundary between cycles A and B (ca. (1) Montney and (2) Doig and Halfway formations).

Fig. 11. Results of the QEMSCAN analyses. (**a**) Ternary diagram of the quartz-feldspar-mica (Q-F-M), carbonates and clay content in the samples, (**b**) quartz versus carbonates cross plot of the analysed samples. Note the two different trends between cycles A and B (ca. Montney and Sunset Prairie formations and Doig and Halfway formations).

Fig. 12. Stratigraphic framework of the Lower and Middle Triassic strata of Western Canada (modified from Davies *et al*., 1997). It presents (**a**) the global eustatic variations (from Hardenbol *et al*., 1998), (**b**) the major stratigraphic observations and (**c**) interpretations from this work together with the (**d**) long- and medium-term of a (**e**) composite eustatic variations curve that corresponds to (**f**) the stratigraphic evolution. This is interpreted as a time gap between the deposition of cycles A and B. Note that on this figure the Induan – Olenekian boundary is placed at 250 Ma as suggested by Henderson *et al.* (2018) while defined at 251.2 Ma by the ICS (Cohen *et al.,* 2013).

628 **REFERENCES**

629 Armitage, J.H. 1962. Triassic Oil and Gas Occurrences in Northeastern British Columbia,
630 Canada. *Bulletin of Canadian Petroleum Geology*, **10**, 35–56.

631 Baby, G., Guillocheau, F., Boulogne, C., Robin, C. & Dall'Asta, M. 2018. Uplift history of a
632 transform continental margin revealed by the stratigraphic record: The case of the
633 Agulhas transform margin along the Southern African Plateau. *Tectonophysics*, **731**–
634 **732**, 104–130, https://doi.org/10.1016/j.tecto.2018.03.014.

635 Barclay, J.E., Krause, F.F., Campbell, R.I. & Utting, J. 1990. Dynamic casting and growth
636 faulting: Dawson Creek graben complex, Carboniferous-Permian Peace River
637 embayment, western Canada. *Bulletin of Canadian Petroleum Geology*, **38**, 115–145.

638 Beranek, L.P. & Mortensen, J.K. 2011. The timing and provenance record of the Late Permian
639 Klondike orogeny in northwestern Canada and arc-continent collision along western
640 North America. *Tectonics*, **30**, https://doi.org/10.1029/2010TC002849.

641 Berger, Z., Boast, M. & Mushayandebvu, M. 2008. The contribution of integrated HRAM
642 studies to exploration and exploitation of unconventional plays in North America.
643 *Reservoir*, **35**, 42–48.

644 Burwash, R.A., McGregor, C.R. & Wilson, J. 1994. Precambrian basement beneath the
645 Western Canada sedimentary basin. *In*: Mossop, G. D. & Shetsen, I. (eds) *Geological*
646 *Atlas of the Western Canadian Sedimentary Basin*. CSPG and Alberta Research Council,
647 49–56.

648 Butcher, G.S., Kendall, A.C., Boyce, A.J., Millar, I.L., Andrews, J.E. & Dennis, P.F. 2012. Age
649 determination of the Lower Watrous red-beds of the Williston Basin, Saskatchewan,
650 Canada. *Bulletin of Canadian Petroleum Geology*, **60**, 227–238,
651 https://doi.org/10.2113/gscpgbull.60.4.227.

652 Cant, D.J. 1988. Regional structure and development of the Peace River Arch, Alberta: A
653 Paleozoic failed-rift system? *Bulletin of Canadian Petroleum Geology*, **36**, 284–295.

654 Carlson, C.E. 1968. Triassic-Jurassic of Alberta, Saskatchewan, Manitoba, Montana, and
655 North Dakota. *AAPG Bulletin*, **52**, 1969–1983.

656 Catuneanu, O. 2006. *Principles of Sequence Stratigraphy*. Elsevier.

657 Catuneanu, O., Abreu, V., et al. 2009. Towards the standardization of sequence stratigraphy.
658 *Earth-Science Reviews*, **92**, 1–33, https://doi.org/10.1016/j.earscirev.2008.10.003.

659 Cohen, K.M., Finney, S.C., Gibbard, P.L. & Fan, J.-X. 2013. *The ICS International*
660 *Chronostratigraphic Chart*, https://doi.org/10.1111/j.1502-3931.1980.tb01026.x.

661 Contreras, J., Zühlke, R., Bowman, S. & Bechstädt, T. 2010. Seismic stratigraphy and
662 subsidence analysis of the southern Brazilian margin (Campos, Santos and Pelotas
663 basins). *Marine and Petroleum Geology*, **27**, 1952–1980,
664 https://doi.org/10.1016/j.marpetgeo.2010.06.007.

665 Crombez, V., Rohais, S., Baudin, F., Chauveau, B., Euzen, T. & Granjeon, D. 2017. Controlling
666 factors on source rock development: implications from 3D stratigraphic modeling of
667 Triassic deposits in the Western Canada Sedimentary Basin. *Bulletin de la Société*
668 *géologique de France*, **188**, 30, https://doi.org/10.1051/bsgf/2017188.

669 Crombez, V., Baudin, F., et al. 2017. Basin scale distribution of organic matter in marine fine-
670 grained sedimentary rocks: Insight from sequence stratigraphy and multi-proxies
671 analysis in the Montney and Doig formations. *Marine and Petroleum Geology*, **83**, 382–
672 401, https://doi.org/10.1016/j.marpetgeo.2016.10.013.

673 Crombez, V., Rohais, S., Baudin, F. & Euzen, T. 2016. Facies, well-log patterns, geometries
674 and sequence stratigraphy of a wave-dominated margin: Insight from the Montney
675 Formation (Alberta, British Columbia, Canada). *Bulletin of Canadian Petroleum Geology*,
676 **64**, 516–537, https://doi.org/10.2113/gscpgbull.64.4.516.

677 Cumming, A.D. 1956. The Watrous strata in Saskatchewan. *In*: *First International Williston*
678 *Basin Symposium*. North Dakota Geol. Society and Saskatchewan Geol. Soc., 165–169.

679 Dai, A. & Trenberth, K.E. 2002. Estimates of Freshwater Discharge from Continents:
680 Latitudinal and Seasonal Variations. *Journal of Hydrometeorology*, **3**, 660–687,
681 https://doi.org/10.1175/1525-7541(2002)003<0660:EOFDFC>2.0.CO;2.

682 Davies, G.R. 1997. The Triassic of the Western Canada Sedimentary Basin: Tectonic and
683 Stratigraphic Framework, Paleogeography, Paleoclimate and Biota. *Bulletin of Canadian*
684 *Petroleum Geology*, **45**, 434–460.

685 Davies, G.R., Moslow, T.F. & Sherwin, M.D. 1997. The Lower Triassic Montney Formation,
686 West-Central Alberta. *Bulletin of Canadian Petroleum Geology*, **45**, 474–505.

687 Dixon, J. 2000. Regional Lithostratigraphic Units in the Triassic Montney Formation of
688 Western Canada: GEOLOGICAL NOTE. *Bulletin of Canadian petroleum geology*, **48**, 80–
689 83.

690 Ducros, M., Sassi, W., Vially, R., Euzen, T. & Crombez, V. 2017. 2-D Basin Modeling of the
691 Western Canada Sedimentary Basin across the Montney-Doig System: Implications for
692 Hydrocarbon Migration Pathways and Unconventional Resources Potential. 117–134,
693 https://doi.org/10.1306/13602027M1143703.

694 Eaton, D.W., Ross, G.M. & Hope, J. 1999. The rise and fall of a cratonic arch : A regional
695 seismic perspective on the Peace River Arch, Alberta. *Bulletin of Canadian petroleum*
696 *geology*, **47**, 346–361.

Edwards, D.E., Barclay, J.E., Gibson, D.W., Kvill, G.E. & Halton, E. 1994. Triassic Strata of the Western Canada Sedimentary Basin. *In*: Mossop, G. D. & Shetsen, I. (eds) *Geological Atlas of the Western Canada Sedimentary Basin*. CSPG and Alberta Research Council, 259–273.

Embry, A.F. 1997. Global Sequence Boundaries of the Triassic and Their Identification in the Western Canada Sedimentary Basin. *Bulletin of Canadian Petroleum Geology*, **45**, 415–433.

Embry, A.F. & Gibson, D.W. 1995. TR sequence analysis of the Triassic succession of the Western Canada Sedimentary Basin. *In*: *Geological Survey of Canada, Open File 3058*. 25–28.

Euzen, T., Moslow, T.F., Crombez, V. & Rohais, S. 2018. Regional stratigraphic architecture of the Spathian Deposits in Western Canada — Implications for the Montney Resource Play T. Euzen, Moslow, T. F. & M. Caplan (eds). *Bulletin of Canadian Petroleum Geology*, **66**, 175–192.

Evoy, R.W. 1995. *The Role of Sediment Bypassing in Siliciclastic Facies Variability on the Continental Shelf: Examples from the Fraser River Delta Foreslope and the Middle Triassic Doig Formation*. PhD Thesis, University of Alberta.

Evoy, R.W. 1997. Lowstand Shorefaces in the Middle Triassic Doig Formation: Implications for Hydrocarbon Exploration in the Fort St. John Area, Northeastern British Columbia. *Bulletin of Canadian Petroleum Geology*, **45**, 537–552.

Evoy, R.W. & Moslow, T.F. 1995. Lithofacies associations and depositional environments in the Middle Triassic Doig Formation, Buick Creek Field, northeastern British Columbia. *Bulletin of Canadian Petroleum Geology*, **43**, 461–475.

Ferri, F. & Zonneveld, J.-P. 2008. Were Triassic rocks of the Western Canada Sedimentary Basin deposited in a foreland. *Canadian Society of Petroleum Geologists Reservoir*, **35**, 12–14.

Furlong, C.M., Gegolick, A., et al. 2018a. Sedimentology and Ichnology of the Middle Triassic (Anisian) Sunset Prairie Formation of the Western Canada Sedimentary Basin T. Euzen, Moslow, T. F. & M. Caplan (eds). *Special Issue of Bulletin of Canadian Petroleum Geology*, **66**, 215–236.

Furlong, C.M., Gingras, M.K., Moslow, T.F. & Zonneveld, J.-P. 2018b. The Sunset Prairie Formation: designation of a new Middle Triassic formation between the Lower Triassic Montney Formation and Middle Triassic Doig Formation in the Western Canada Sedimentary Basin, northeast British Columbia. Euzen, T., Moslow, T. F. & Caplan, M. (eds). *Bulletin of*, **66**, 193–214.

Gibson, D.W. 1975. *Triassic Rocks of the Rocky Mountain Foothills and Front Ranges of Northeastern British Columbia and West-Central Alberta*. Geological Survey of Canada, Bulletin 247.Gibson, D.W. & Barclay, J.E. 1989. Middle Absaroka Sequence - The Triassic

735 Stable Craton. *Western Canada Sedimentary Basin - a Case History, Special Publication*,
736 **30**, 219–232, https://doi.org/10.1037/0022-3514.84.2.377.

737 Gibson, D.W. 1974. *Triassic Rocks of the Southern Canadian Rocky Mountains*. Geological
738 Survey of Canada, Bulletin 247.

739 Golding, M.L., Mortensen, J.K., Ferri, F., Zonneveld, J.-P. & Orchard, M. 2015a. Determining
740 the provenance of Triassic sedimentary rocks in northeastern British Columbia and
741 western Alberta using detrital zircon geochronology, with implications for regional
742 tectonics. *Canadian Journal of Earth Sciences*, **53**, 140–155,
743 https://doi.org/10.1139/cjes-2015-0082.

744 Golding, M.L., Mortensen, J.K., Zonneveld, J.P. & Orchard, M.J. 2016. U-Pb isotopic ages of
745 euhedral zircons in the Rhaetian of British Columbia: Implications for Cordilleran
746 tectonics during the Late Triassic. *Geosphere*, https://doi.org/10.1130/GES01324.1.

747 Golding, M.L., Orchard, M.J., Zonneveld, J.-P., Henderson, C.M. & Dunn, L. 2014. An
748 exceptional record of the sedimentology and biostratigraphy of the Montney and Doig
749 formations in British Columbia. *Bulletin of Canadian Petroleum Geology*, **62**, 157–176.

750 Golding, M.L., Orchard, M.J., Zonneveld, J.-P. & Wilson, N.S.F. 2015b. Determining the age
751 and depositional model of the Doig Phosphate Zone in northeastern British Columbia
752 using conodont biostratigraphy. *Bulletin of Canadian Petroleum Geology*, **63**, 143–170.

753 Golonka, J., Ross, M.I. & Scotese, C.R. 1994. Phanerozoic paleogeographic and paleoclimatic
754 modeling maps. *In*: *Pangea: Global Environments and Resources*. CSPG Special
755 Publications.

756 Gottlieb, P., Wilkie, G., et al. 2000. Using quantitative electron microscopy for process
757 mineralogy applications. *JOM*, **52**, 24–25, https://doi.org/10.1007/s11837-000-0126-9.

758 Grimaud, J.L., Rouby, D., Chardon, D. & Beauvais, A. 2018. Cenozoic sediment budget of
759 West Africa and the Niger delta. *Basin Research*, https://doi.org/10.1111/bre.12248.

760 Guillocheau, F., Chelalou, R., et al. 2015. Cenozoic landscape evolution in and around the
761 Congo Basin: Constraints from sediments and planation surfaces. *In*: *Geology and*
762 *Resource Potential of the Congo Basin*. 1–417., https://doi.org/10.1007/978-3-642-
763 29482-2_14.

764 Guillocheau, F., Rouby, D., Robin, C., Helm, C., Rolland, N., Le Carlier de Veslud, C. & Braun, J.
765 2012. Quantification and causes of the terrigeneous sediment budget at the scale of a
766 continental margin: A new method applied to the Namibia-South Africa margin. *Basin*
767 *Research*, **24**, 3–30, https://doi.org/10.1111/j.1365-2117.2011.00511.x.

768 Hallam, A. 1985. A review of Mesozoic climates. *Journal of the Geological Society*, **142**, 433–
769 445, https://doi.org/10.1144/gsjgs.142.3.0433.

Haq, B.U., Hardenbol, J. & Vail, P.R. 1987. Chronology of Fluctuating Sea Levels Since the Triassic. *Science*, **235**, 1156–1167, https://doi.org/10.1126/science.235.4793.1156.

Hardenbol, J., Thierry, J., Farley, M., Jacquin, T., De Graciansky, P.C. & Vail, P.R. 1998. Mesozoic and Cenozoic Sequence Chronostratigraphic Framework of European Basins. *In*: P.-C.D. Graciansky, J. Hardenbol, T. J. and P. R. V. (ed.) *European Basins. In Mesozoic and Cenozoic Sequence Stratigraphy of European Basins*. Special Publications of SEPM N°60, 3–13.

Harris, R.G. 2000. *Triassic Doig Formation Sand Bodies in the Peace River Area of Western Canada : Depositional and Structural Models, and the Impact of Diagenesis on Reservoir Properties*. MSc Thesis, University of British Columbia., https://doi.org/10.1007/s13398-014-0173-7.2.

Helland-Hansen, W. & Gjelberg, J.G. 1994. Conceptual basis and variability in sequence stratigraphy: a different perspective. *Sedimentary Geology*, **92**, 31–52, https://doi.org/10.1016/0037-0738(94)90053-1.

Helland-Hansen, W. & Hampson, G.J. 2009. Trajectory analysis: concepts and applications. *Basin Research*, **21**, 454–483, https://doi.org/10.1111/j.1365-2117.2009.00425.x.

Helland-Hansen, W. & Martinsen, O.J. 1996. Shoreline trajectories and sequences; description of variable depositional-dip scenarios. *Journal of Sedimentary Research*, **66**, 670–688, https://doi.org/10.1306/D42683DD-2B26-11D7-8648000102C1865D.

Henderson, C.M., Golding, M.L. & Orchard, M.J. 2018. Conodont Sequence Biostratigraphy of the Lower Triassic Montney Formation Euzen, T., Moslow, T. F. & M. Caplan (eds). *Special Issue of Bulletin of Canadian Petroleum Geology*, **66**, 7–22.

Henderson, C.M. & Schoepfer, S.D. 2017. High-Resolution Biostratigraphic and XRF585 Geochemical Correlation of the Montney Formation, NEBC. *In*: *CSPG CSEG CWLS Join Annual Convention*. Calgary.

Hoffman, P.F. 1987. Continental transform tectonics: Great Slave Lake shear zone (ca. 1.9 Ga), northwest Canada. *Geology*, **15**, 785–788, https://doi.org/10.1130/0091-7613(1987)15.

Hunt, D. & Tucker, M.E. 1992. Stranded parasequences and the forced regressive wedge systems tract: deposition during base-level fall—reply. *Sedimentary Geology*, **95**, 147–160, https://doi.org/10.1016/0037-0738(94)00123-C.

Kendall, D.R. 1999. *Sedimentology and Stratigraphy of the Lower Triassic Montney Formation, Peace River Basin, Subsurface of Northwestern Alberta*. MSc Thesis, University of Calgary.

Kent, D.M. 1994. Paleogeographic evolution of the cratonic platform-Cambrian to Triassic. *In*: Shetsen, G. M. and I. (ed.) *Geological Atlas of the Western Canada Sedimentary Basin, G. Mossop and I. Shetsen, Compilers, Canadian Society of Petroleum Geologists*

807 *and Alberta Research Council, Special Report*. CSPG and Alberta Research Council, 69–
808 86.

809 Leroux, E., Rabineau, M., et al. 2017. High-resolution evolution of terrigenous sediment
810 yields in the Provence Basin during the last 6 Ma: relation with climate and tectonics.
811 *Basin Research*, **29**, 305–339, https://doi.org/10.1111/bre.12178.

812 Markhasin, B. 1997. *Sedimentology and Stratigraphy of the Lower Triassic Montney*
813 *Formation, Subsurface of Northwestern Alberta*. MSc Thesis, University of Calgary.

814 Martinsen, O.J., Sømme, T.O., Thurmond, J.B., Helland-Hansen, W. & Lunt, I. 2010. Source-
815 to-sink systems on passive margins: theory and practice with an example from the
816 Norwegian continental margin. *In*: *Petroleum Geology: From Mature Basins to New*
817 *Frontiers—Proceedings of the 7th Petroleum Geology Conference*. 913–920.,
818 https://doi.org/10.1144/0070913.

819 Matenco, L., Andriessen, P., et al. 2013. Quantifying the mass transfer from mountain ranges
820 to deposition in sedimentary basins: Source to sink studies in the Danube basin-black
821 sea system. *Global and Planetary Change*, **103**, 1–18,
822 https://doi.org/10.1016/j.gloplacha.2013.01.003.

823 McMechan, M.E. 1990. Upper Proterozoic to Middle Cambrian history of the Peace River
824 arch: evidence from the Rocky Mountains. *Bulletin of Canadian Petroleum Geology*, **38**,
825 36–44.

826 Miall, A.D. 1986. Eustatic sea level changes interpreted from seismic stratigraphy: a critique
827 of the methodology with particular reference to the North Sea Jurassic record.
828 *American Association of Petroleum Geologists Bulletin*,
829 https://doi.org/10.1306/9488593A-1704-11D7-8645000102C1865D.

830 Miall, A.D. 2009. Correlation of sequences and the global eustasy paradigm: A review of
831 current data. *In*: *Geoconvention: Frontiers+ Innovation*. 123–126.

832 Milliman, J.D. & Meade, R.H. 1983. World-Wide Delivery of River Sediment to the Oceans.
833 *The Journal of Geology*, **91**, 1–21.

834 Monger, J. & Price, R. 2002. The Canadian cordillera: Geology and Tectonic Evolution. *CSEG*
835 *Recorder*, **27**, 17–36.

836 Morris, N., Asgar-Deen, M., Gardner, D. & Glemser, C. 2018. A Preliminary Investigation of
837 the Igneous Origins of the Montney and Doig formations: Integrating Igneous
838 Geochemistry Techniques for Interpreting Sedimentary Provenance. *Bulletin of*
839 *Canadian Petroleum Geology*, **66**, 161–174.

840 Moslow, T.F. & Davies, G.R. 1997. Turbidite Reservoir Facies in the Lower Triassic Montney
841 Formation, West-Central Alberta. *Bulletin of Canadian Petroleum Geology*, **45**, 507–536.

842 Moslow, T.F. & Zaitlin, B.A. 2008. Tight Gas Reservoirs of the Western Canada Deep Basin. *In*:
843 *AAPG Annual Convention*. San Antonio.

844 O'connell, S.C. 1994. Geological history of the Peace River arch. *In*: GD Mossop and I.
845 Shetsen (ed.) *Geological Atlas of the Western Canada Sedimentary Basin*. CSPG and
846 Alberta Research Council, 431–437.

847 O'Connell, S.C., Dix, G.R. & Barclay, J.E. 1990. The origin, history, and regional structural
848 development of the Peace River Arch, Western Canada. *Bulletin of Canadian Petroleum*
849 *Geology*, **38**, 4–24.

850 Onoue, T., Zonneveld, J.-P., Orchard, M.J., Yamashita, M., Yamashita, K., Sato, H. & Kusaka, S.
851 2016. Paleoenvironmental changes across the Carnian/Norian boundary in the Black
852 Bear Ridge section, British Columbia, Canada. *Palaeogeography, Palaeoclimatology,*
853 *Palaeoecology*, **441**, 721–733, https://doi.org/10.1016/j.palaeo.2015.10.008.

854 Orchard, M.J. & Tozer, E.T. 1997. Triassic conodont biochronology, its calibration with the
855 ammonoid standard, and a biostratigraphic summary for the Western Canada
856 Sedimentary Basin. *Bulletin of Canadian Petroleum Geology*, **45**, 675–692.

857 Orchard, M.J. & Zonneveld, J.-P. 2009. The Lower Triassic Sulphur Mountain Formation in the
858 Wapiti Lake area: lithostratigraphy, conodont biostratigraphy, and a new biozonation
859 for the lower Olenekian (Smithian). *Canadian Journal of Earth Sciences*, **46**, 757–790.

860 Panek, R. 2000. *The Sedimentology and Stratigraphy of the Lower Triassic Montney*
861 *Formation in the Subsurface of the Peace River Area, Northwestern Alberta*. MSc Thesis,
862 University of Calgary.

863 Playter, T., Corlett, H., et al. 2018. Clinoform identification and correlation in fine-grained
864 sediments: A case study using the Triassic Montney Formation. *Sedimentology*, **65**, 263–
865 302, https://doi.org/10.1111/sed.12403.

866 Posamentier, H.W. & Walker, R.G. (eds). 2006. *Facies Models Revisited*. Special Publications
867 of SEPM.

868 Power, M.R. & Burns, S. 2013. The Comparison of QEMSCAN and XRD Analysis in the
869 Mineralogical Characterisation of Unconventional Reservoirs: The Benefits of an
870 Integrated Approach. *In*: *CSPG CSEG CWLS Join Annual Convention*. Calgary.

871 Price, R.A. 1994. Cordilleran tectonics and the evolution of the Western Canada Sedimentary
872 Basin. *In*: Mossop, G. D. & Shetsen, I. (eds) *Geological Atlas of the Western Canada*
873 *Sedimentary Basin*. CSPG and Alberta Research Council, 13–24.

874 Price, R.A., Balkwill, H.R., Charlesworth, H.A.K., Cook, D.G. & Simony, P.S. 1972. The
875 Canadian Rockies and tectonic evolution of the southeastern Canadian Cordillera: 24th
876 International Geological Congress. *Guidebook for Excursion A15-C15, Geological Survey*
877 *of Canada*.

878 Reed Jr., J.C., Wheeler, J.O. & Tucholke, B.E. 2005. *Decade of North American Geology*
879 *Geologic Map of North America—Perspectives and Explanation*,
880 https://doi.org/10.1130/DNAG-CSMS-v1.1.

881 Rohais, S., Barrois, A., Colletta, B. & Moretti, I. 2016. Pre-salt to salt stratigraphic
882 architecture in a rift basin: insights from a basin-scale study of the Gulf of Suez (Egypt).
883 *Arabian Journal of Geosciences*, **9**, 24p, https://doi.org/10.1007/s12517-016-2327-8.

884 Rohais, S., Crombez, V., Euzen, T. & Zonneveld, J.-P. 2018. Subsidence dynamics of the
885 Montney Formation (Early Triassic, Western Canada Sedimentary Basin): insights for its
886 geodynamic setting and wider implications Euzen, T., Moslow, T. F. & Caplan, M. (eds).
887 *Bulletin of Canadian Petroleum Geology*, **66**, 128–160.

888 Ross, G.M. 1990. Deep crust and basement structure of the Peace River Arch region:
889 constraints on mechanisms of formation. *Bulletin of Canadian Petroleum Geology*, **38**,
890 25–35.

891 Rouby, D., Bonnet, S., et al. 2009. Sediment supply to the Orange sedimentary system over
892 the last 150 My: An evaluation from sedimentation/denudation balance. *Marine and*
893 *Petroleum Geology*, **26**, 782–794, https://doi.org/10.1016/j.marpetgeo.2008.08.004.

894 Sellwood, B.W. & Valdes, P.J. 2006. Mesozoic climates: General circulation models and the
895 rock record. *Sedimentary Geology*, **190**, 269–287,
896 https://doi.org/10.1016/j.sedgeo.2006.05.013.

897 Sturrock, D.L. & Dawson, S.W. 1990. Ring/Border Field, Alberta and British Columbia. *Oil and*
898 *Gas Pools of Canada Series*, **1**.

899 Suter, E.H. 2006. Facies Models Revisited: Clastic Shelves. *In*: Posamentier, H. W. & Walker,
900 R. G. (eds) *Facies Models Revisited*. SEPM Special Publication N°84, 339–398.

901 Switzer, S.B., Holland, W.G., et al. 1994. Devonian Woodbend-Winterburn strata of the
902 Western Canada sedimentary basin. *In*: Shetsen, G. M. and I. (ed.) *Geological Atlas of*
903 *the Western Canada Sedimentary Basin*. CSPG and Alberta Research Council, 165–202.

904 Vaisblat, N., Harris, N.B., DeBhur, C., Euzen, T., Gasparrini, M., Crombez, V., Rohais, S.,
905 Krause, F., Ayranci, K., 2017. Diagenetic model for the deep Montney Formation,
906 northeastern British Columbia. Geoscience BC Summary of Activities 2016, Geoscience
907 BC, Report 2017-1, 37–48.

908 Wright, G.N., McMechan, M.E. & Potter, D.E.G. 1994. Structure and Architecture of the
909 Western Canada Sedimentary Basin. *In*: Mossop, G. D. & Shetsen, I. (eds) *Geological*
910 *Atlas of the Western Canada Sedimentary Basin*. CSPG and Alberta Research Council,
911 25–40.

912 Zonneveld, J.-P. 2000. *Sedimentology and Sequence Biostratigraphic Framework of a Mixed*
913 *Siliciclastic-Carbonate Depositional System, Middle Triassic, Northeastern British*
914 *Columbia*. PhD Thesis, University of Alberta.

915 Zonneveld, J.-P. 2001. Middle Triassic biostromes from the Liard Formation, British
916 Columbia, Canada: oldest examples from the Mesozoic of NW Pangea. *Sedimentary*
917 *Geology*, **145**, 317–341.

918 Zonneveld, J.-P., Gingras, M.K. & Beatty, T.W. 2010. Diverse ichnofossil assemblages
919 following the PT mass extinction, Lower Triassic, Alberta and British Columbia, Canada:
920 evidence for shallow marine refugia on the northwestern coast of Pangaea. *Palaios*, **25**,
921 368–392.

922 Zonneveld, J.-P., Gingras, M.K. & Pemberton, S.G. 2001. Trace fossil assemblages in a Middle
923 Triassic mixed siliciclastic-carbonate marginal marine depositional system, British
924 Columbia. *Palaeogeography, Palaeoclimatology, Palaeoecology*, **166**, 249–276.

925 Zonneveld, J.-P., MacNaughton, R.B., Utting, J., Beatty, T.W., Pemberton, S.G. & Henderson,
926 C.M. 2010. Sedimentology and Ichnology of the Lower Triassic Montney Formation in
927 the Pedigree-Ring/Border-Kahntah River Area, Northwestern Alberta and Northeastern
928 British Columbia. *Bulletin of Canadian Petroleum Geology*, **58**, 115–140.

929 Zonneveld, J.-P. & Moslow, T.F. 2014. Perennial River Deltas of the Montney Formation:
930 Alberta and British Columbia Subcrop Edge. *In*: *Geoconvention: Focus*.

931 Zonneveld, J.-P. & Moslow, T.F. 2018. Palaeogeographic setting, Lithostratigraphy, and
932 Sedimentary Framework of the Lower Triassic Montney Formation of western Alberta
933 and northeastern British Columbia Euzen, T., Moslow, T. F. & Caplan, M. (eds). *Bulletin*
934 *of Canadian Petroleum Geology*.

935 Zonneveld, J.-P., Moslow, T.F. & Henderson, C.M. 1997. Lithofacies associations and
936 depositional environments in a mixed siliciclastic-carbonate coastal depositional
937 system, upper Liard Formation, Triassic, northeastern British Columbia. *Bulletin of*
938 *Canadian Petroleum Geology*, **45**, 553–575.

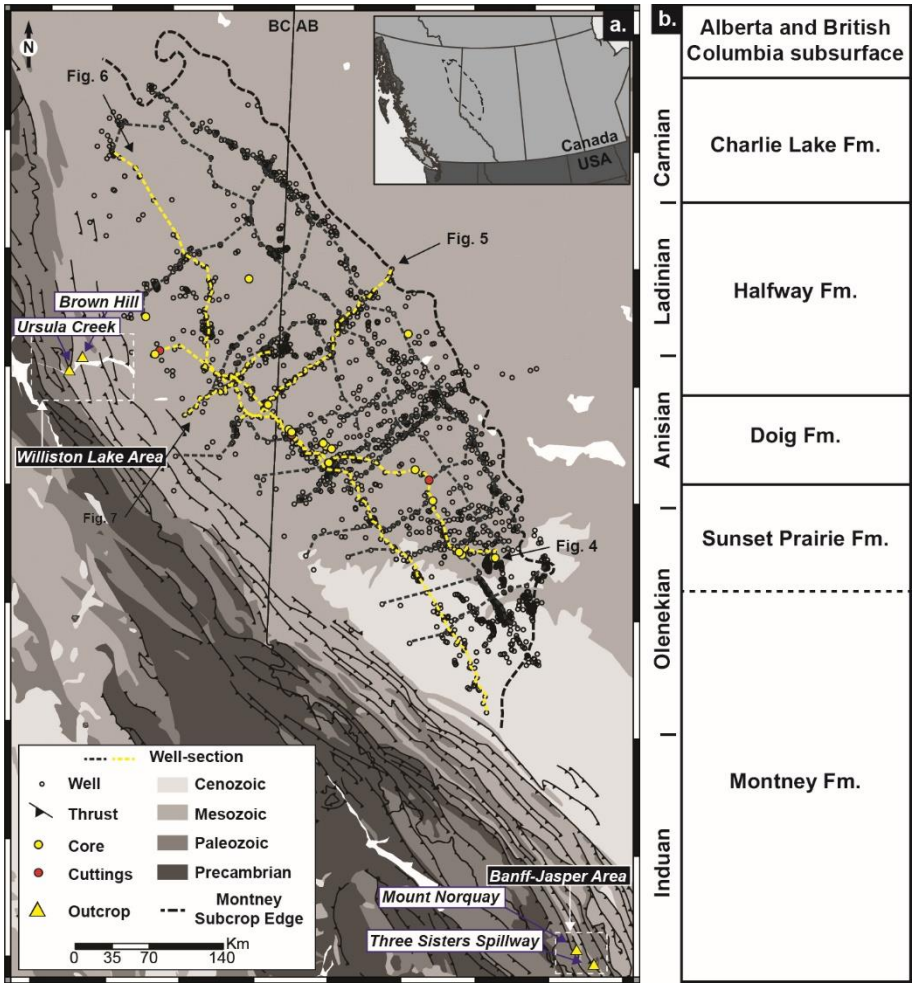
a.
BC AB
N
Fig. 6
Canada
USA
Fig. 5
Brown Hill
Ursula Creek
Williston Lake Area
Fig. 7
Fig. 4
Banff-Jasper Area
Mount Norquay
Three Sisters Spillway
Well-section
Well
Thrust
Core
Cuttings
Outcrop
Cenozoic
Mesozoic
Paleozoic
Precambrian
Montney Subcrop Edge
Km
0 35 70 140
b.
Alberta and British Columbia subsurface
Carnian
Ladinian
Anisian
Olenekian
Induan
Charlie Lake Fm.
Halfway Fm.
Doig Fm.
Sunset Prairie Fm.
Montney Fm.

Figure 1

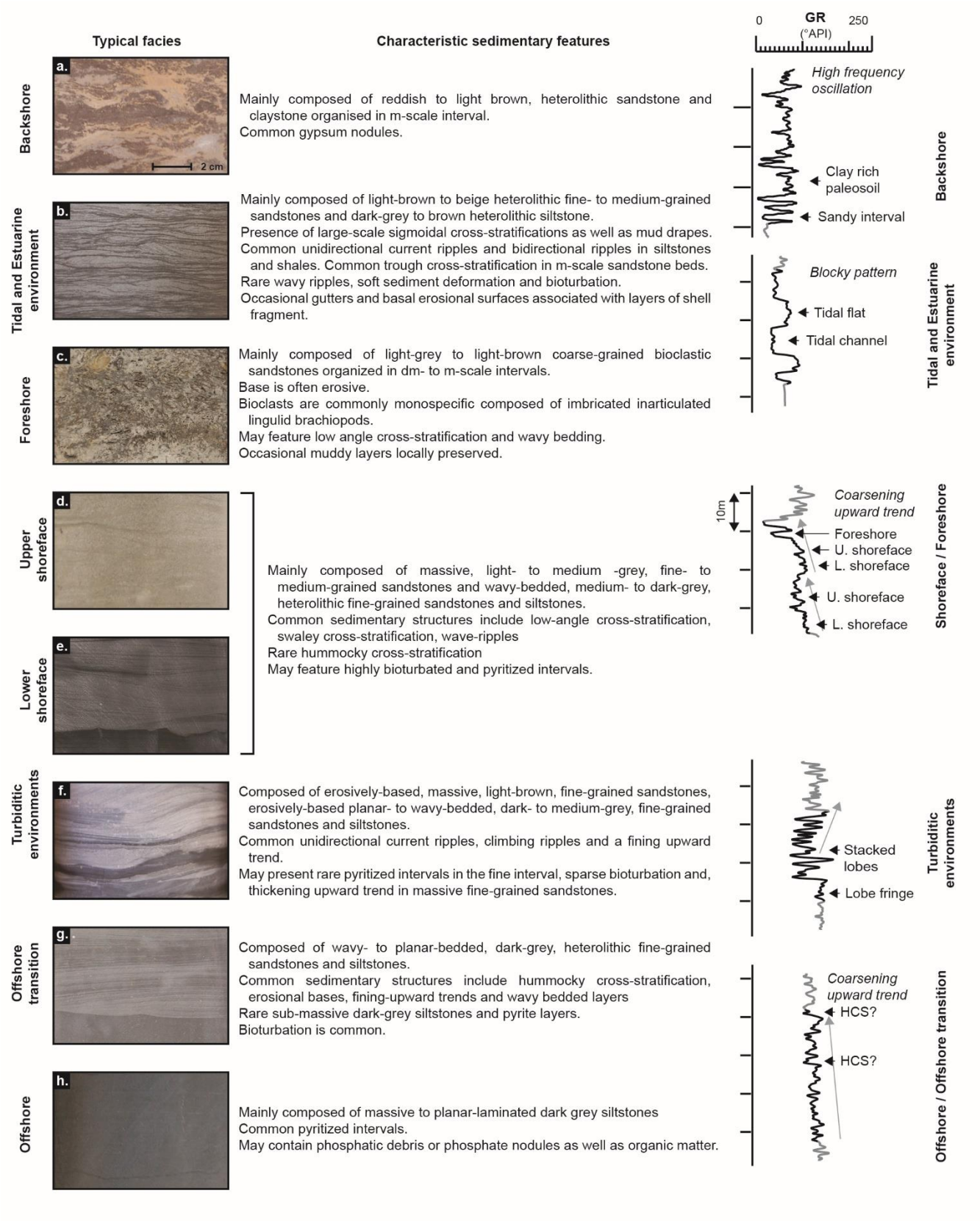
Typical facies
Characteristic sedimentary features
0
GR
250
(°API)
Backshore
a.
2 cm
Mainly composed of reddish to light brown, heterolithic sandstone and claystone organised in m-scale interval.
Common gypsum nodules.
High frequency oscillation
Clay rich paleosoil
Sandy interval
Backshore
Tidal and Estuarine environment
b.
Mainly composed of light-brown to beige heterolithic fine- to medium-grained sandstones and dark-grey to brown heterolithic siltstone.
Presence of large-scale sigmoidal cross-stratifications as well as mud drapes.
Common unidirectional current ripples and bidirectional ripples in siltstones and shales. Common trough cross-stratification in m-scale sandstone beds.
Rare wavy ripples, soft sediment deformation and bioturbation.
Occasional gutters and basal erosional surfaces associated with layers of shell fragment.
Blocky pattern
Tidal flat
Tidal channel
Tidal and Estuarine environment
Foreshore
c.
Mainly composed of light-grey to light-brown coarse-grained bioclastic sandstones organized in dm- to m-scale intervals.
Base is often erosive.
Bioclasts are commonly monospecific composed of imbricated inarticulated lingulid brachiopods.
May feature low angle cross-stratification and wavy bedding.
Occasional muddy layers locally preserved.
Upper shoreface
d.
Lower shoreface
e.
Mainly composed of massive, light- to medium -grey, fine- to medium-grained sandstones and wavy-bedded, medium- to dark-grey, heterolithic fine-grained sandstones and siltstones.
Common sedimentary structures include low-angle cross-stratification, swaley cross-stratification, wave-ripples
Rare hummocky cross-stratification
May feature highly bioturbated and pyritized intervals.
10m
Coarsening upward trend
Foreshore
U. shoreface
L. shoreface
U. shoreface
L. shoreface
Shoreface / Foreshore
Turbiditic environments
f.
Composed of erosively-based, massive, light-brown, fine-grained sandstones, erosively-based planar- to wavy-bedded, dark- to medium-grey, fine-grained sandstones and siltstones.
Common unidirectional current ripples, climbing ripples and a fining upward trend.
May present rare pyritized intervals in the fine interval, sparse bioturbation and, thickening upward trend in massive fine-grained sandstones.
Stacked lobes
Lobe fringe
Turbiditic environments
Offshore transition
g.
Composed of wavy- to planar-bedded, dark-grey, heterolithic fine-grained sandstones and siltstones.
Common sedimentary structures include hummocky cross-stratification, erosional bases, fining-upward trends and wavy bedded layers
Rare sub-massive dark-grey siltstones and pyrite layers.
Bioturbation is common.
Coarsening upward trend
HCS?
HCS?
Offshore / Offshore transition
Offshore
h.
Mainly composed of massive to planar-laminated dark grey siltstones
Common pyritized intervals.
May contain phosphatic debris or phosphate nodules as well as organic matter.

Figure 2

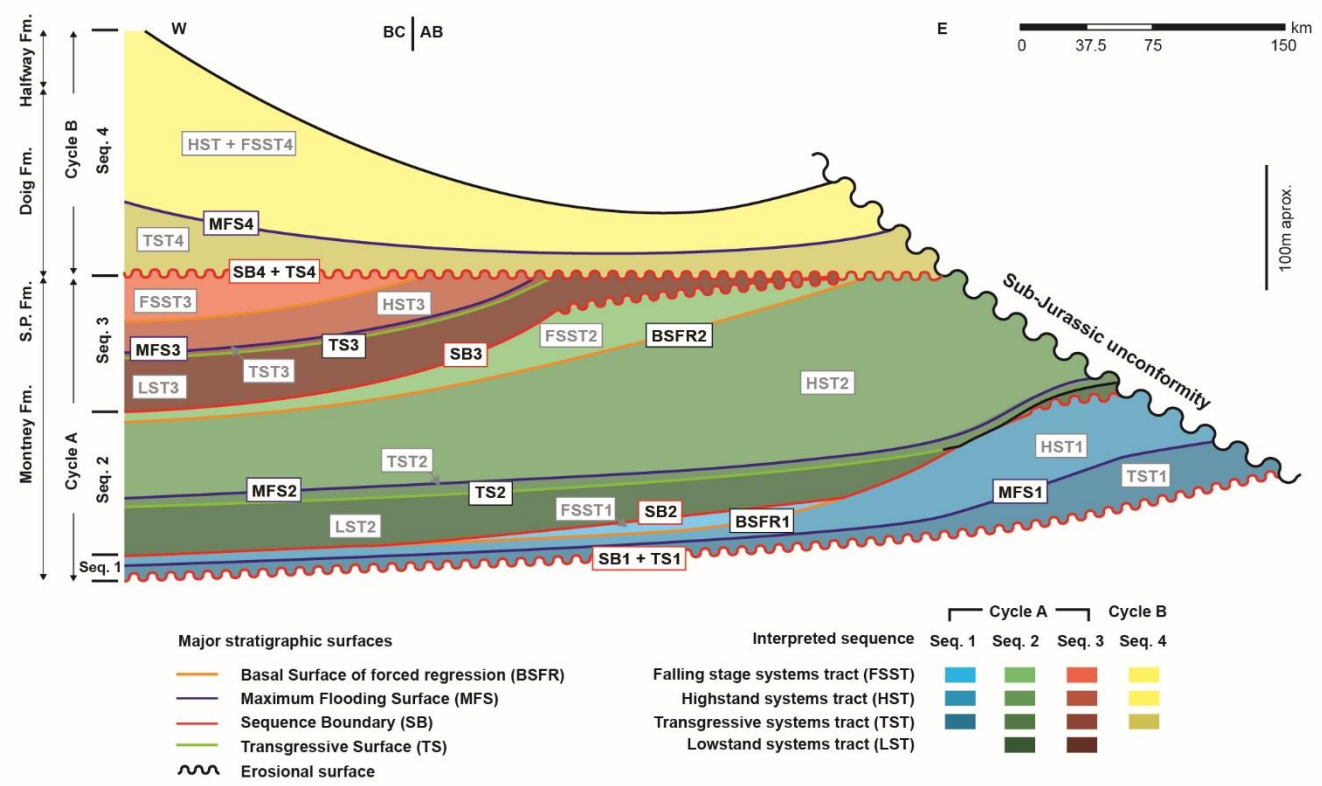
W
BC | AB
E
km
0
37.5
75
150
Halfway Fm.
Doig Fm.
S.P. Fm.
Montney Fm.
Cycle B
Cycle A
Seq. 4
Seq. 3
Seq. 2
Seq. 1
HST + FSST4
TST4
MFS4
SB4 + TS4
FSST3
HST3
MFS3
TS3
TST3
SB3
FSST2
BSFR2
LST3
HST2
Sub-Jurassic unconformity
100m aprox.
TST2
MFS2
TS2
FSST1
SB2
BSFR1
LST2
HST1
TST1
MFS1
SB1 + TS1
Major stratigraphic surfaces
Basal Surface of forced regression (BSFR)
Maximum Flooding Surface (MFS)
Sequence Boundary (SB)
Transgressive Surface (TS)
Erosional surface
Interpreted sequence
Cycle A
Cycle B
Seq. 1
Seq. 2
Seq. 3
Seq. 4
Falling stage systems tract (FSST)
Highstand systems tract (HST)
Transgressive systems tract (TST)
Lowstand systems tract (LST)

Figure 3

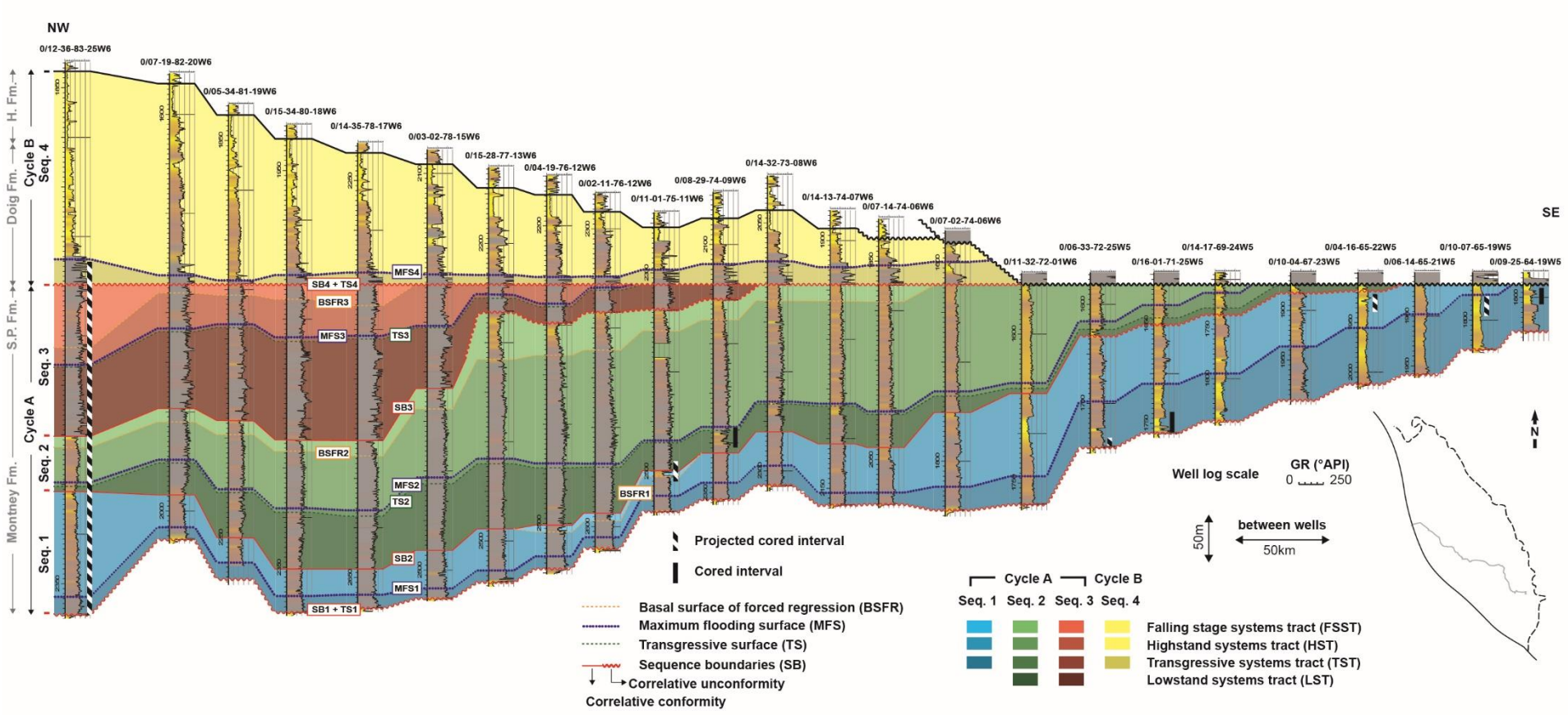
NW
SE
0/12-36-83-25W6
0/07-19-82-20W6
0/05-34-81-19W6
0/15-34-80-18W6
0/14-35-78-17W6
0/03-02-78-15W6
0/15-28-77-13W6
0/04-19-76-12W6
0/02-11-76-12W6
0/11-01-75-11W6
0/08-29-74-09W6
0/14-32-73-08W6
0/14-13-74-07W6
0/07-14-74-06W6
0/07-02-74-06W6
0/11-32-72-01W6
0/06-33-72-25W5
0/16-01-71-25W5
0/14-17-69-24W5
0/10-04-67-23W5
0/04-16-65-22W5
0/06-14-65-21W5
0/10-07-65-19W5
0/09-25-64-19W5
H. Fm.
Doig Fm.
S.P. Fm.
Montney Fm.
Cycle B
Cycle A
Seq. 4
Seq. 3
Seq. 2
Seq. 1
MFS4
SB4 + TS4
BSFR3
MFS3
TS3
SB3
BSFR2
MFS2
TS2
BSFR1
SB2
MFS1
SB1 + TS1
Projected cored interval
Cored interval
Basal surface of forced regression (BSFR)
Maximum flooding surface (MFS)
Transgressive surface (TS)
Sequence boundaries (SB)
Correlative unconformity
Correlative conformity
Well log scale
GR (°API)
0
250
50m
between wells
50km
N
Cycle A
Cycle B
Seq. 1
Seq. 2
Seq. 3
Seq. 4
Falling stage systems tract (FSST)
Highstand systems tract (HST)
Transgressive systems tract (TST)
Lowstand systems tract (LST)

Figure 4

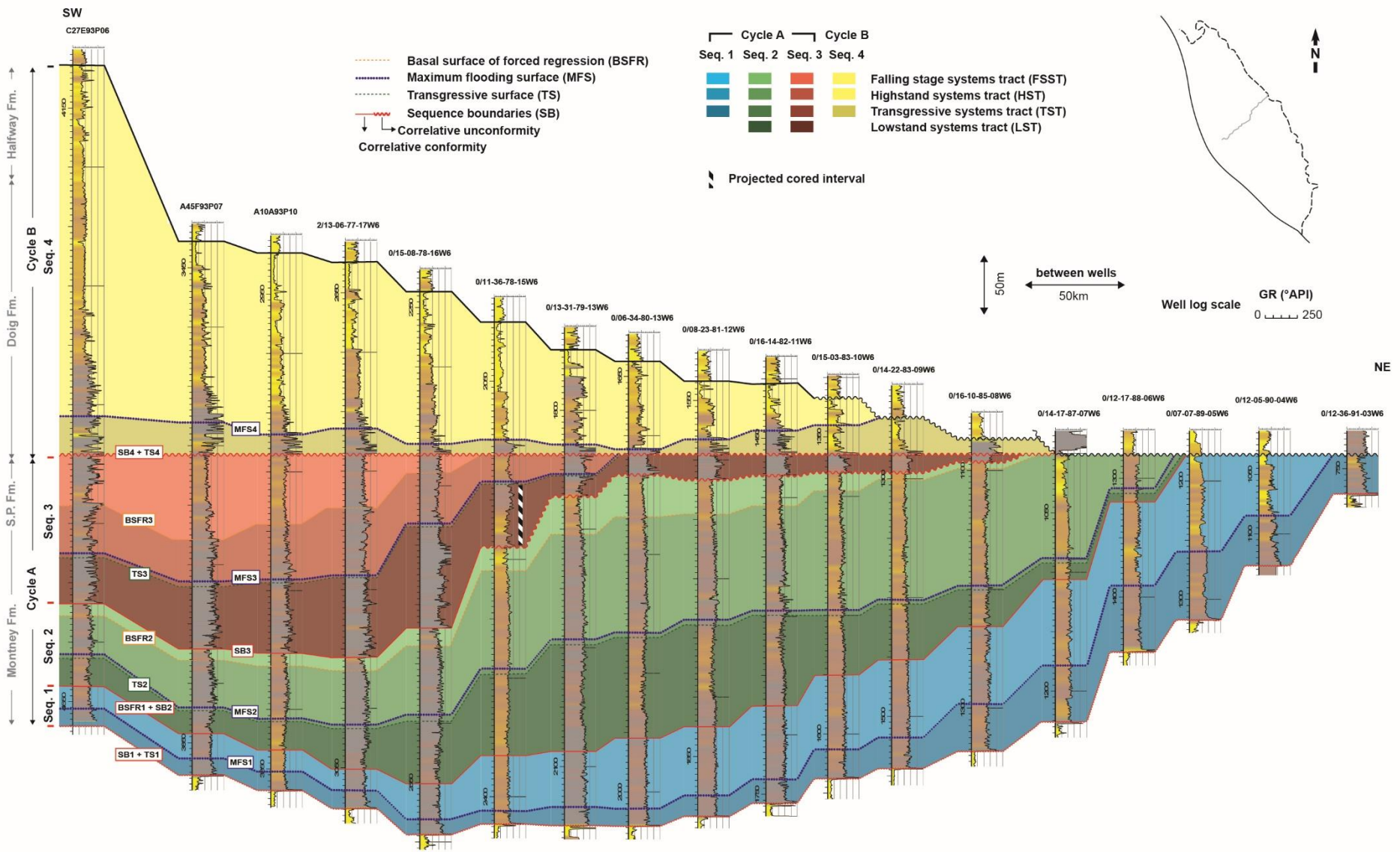
SW
NE
C27E93P06
A45F93P07
A10A93P10
2/13-06-77-17W6
0/15-08-78-16W6
0/11-36-78-15W6
0/13-31-79-13W6
0/06-34-80-13W6
0/08-23-81-12W6
0/16-14-82-11W6
0/15-03-83-10W6
0/14-22-83-09W6
0/16-10-85-08W6
0/14-17-87-07W6
0/12-17-88-06W6
0/07-07-89-05W6
0/12-05-90-04W6
0/12-36-91-03W6
Basal surface of forced regression (BSFR)
Maximum flooding surface (MFS)
Transgressive surface (TS)
Sequence boundaries (SB)
Correlative unconformity
Correlative conformity
Cycle A
Cycle B
Seq. 1
Seq. 2
Seq. 3
Seq. 4
Falling stage systems tract (FSST)
Highstand systems tract (HST)
Transgressive systems tract (TST)
Lowstand systems tract (LST)
Projected cored interval
N
50m
between wells
50km
Well log scale
GR (°API)
0
250
Montney Fm.
Doig Fm.
Halfway Fm.
S.P. Fm.
Cycle A
Cycle B
Seq. 1
Seq. 2
Seq. 3
Seq. 4
SB1 + TS1
BSFR1 + SB2
TS2
BSFR2
SB3
TS3
BSFR3
SB4 + TS4
MFS1
MFS2
MFS3
MFS4

Figure 5

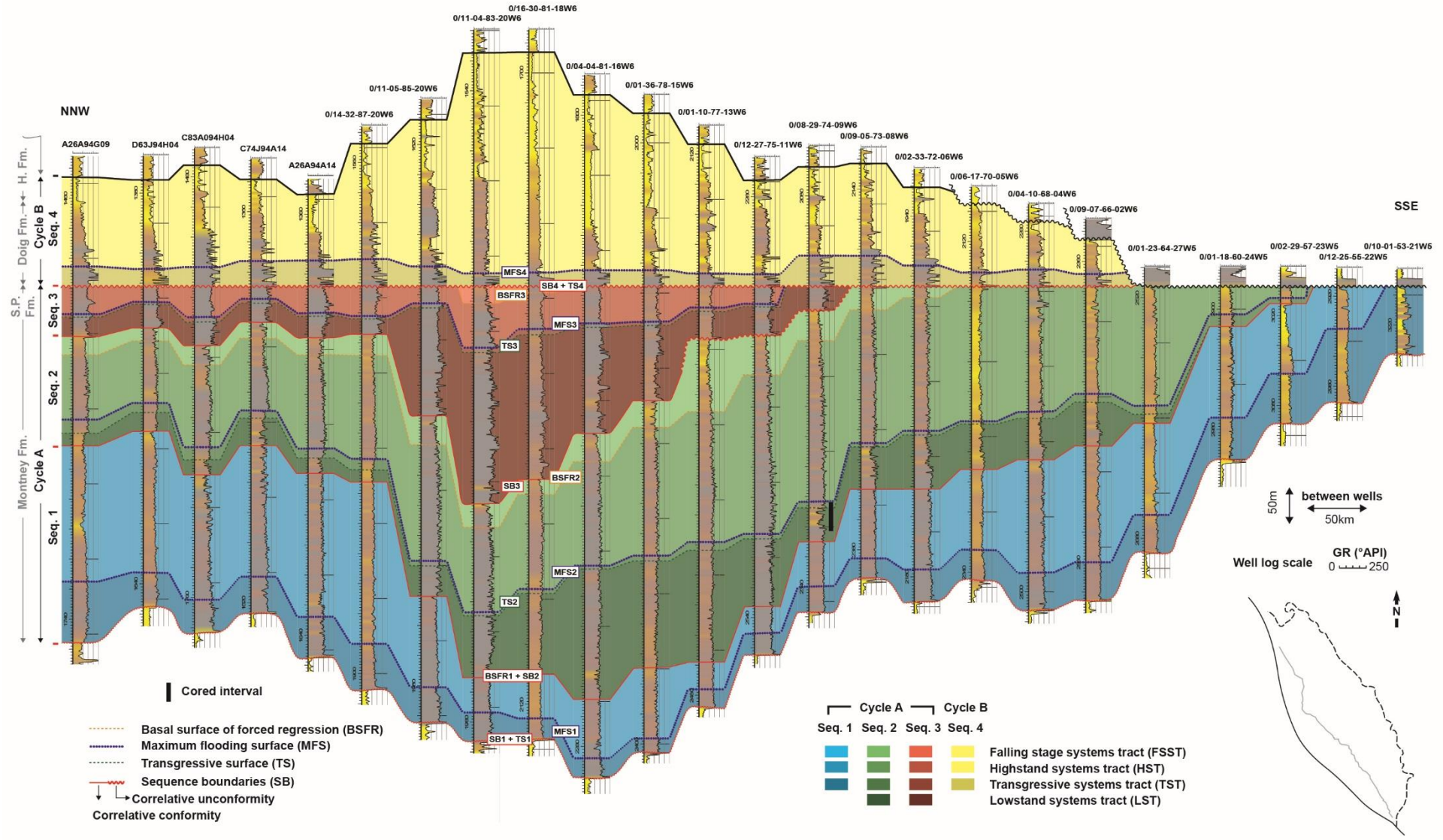
NNW
SSE
A26A94G09
D63J94H04
C83A094H04
C74J94A14
A26A94A14
0/14-32-87-20W6
0/11-05-85-20W6
0/11-04-83-20W6
0/16-30-81-18W6
0/04-04-81-16W6
0/01-36-78-15W6
0/01-10-77-13W6
0/12-27-75-11W6
0/08-29-74-09W6
0/09-05-73-08W6
0/02-33-72-06W6
0/06-17-70-05W6
0/04-10-68-04W6
0/09-07-66-02W6
0/01-23-64-27W5
0/01-18-60-24W5
0/02-29-57-23W5
0/12-25-55-22W5
0/10-01-53-21W5
H. Fm.
Doig Fm.
S.P. Fm.
Montney Fm.
Cycle B
Cycle A
Seq. 4
Seq. 3
Seq. 2
Seq. 1
MFS4
SB4 + TS4
BSFR3
MFS3
TS3
SB3
BSFR2
MFS2
TS2
BSFR1 + SB2
SB1 + TS1
MFS1
50m
between wells
50km
Well log scale
GR (°API)
0
250
N
Cored interval
Basal surface of forced regression (BSFR)
Maximum flooding surface (MFS)
Transgressive surface (TS)
Sequence boundaries (SB)
Correlative unconformity
Correlative conformity
Cycle A
Cycle B
Seq. 1 Seq. 2 Seq. 3 Seq. 4
Falling stage systems tract (FSST)
Highstand systems tract (HST)
Transgressive systems tract (TST)
Lowstand systems tract (LST)

Figure 6

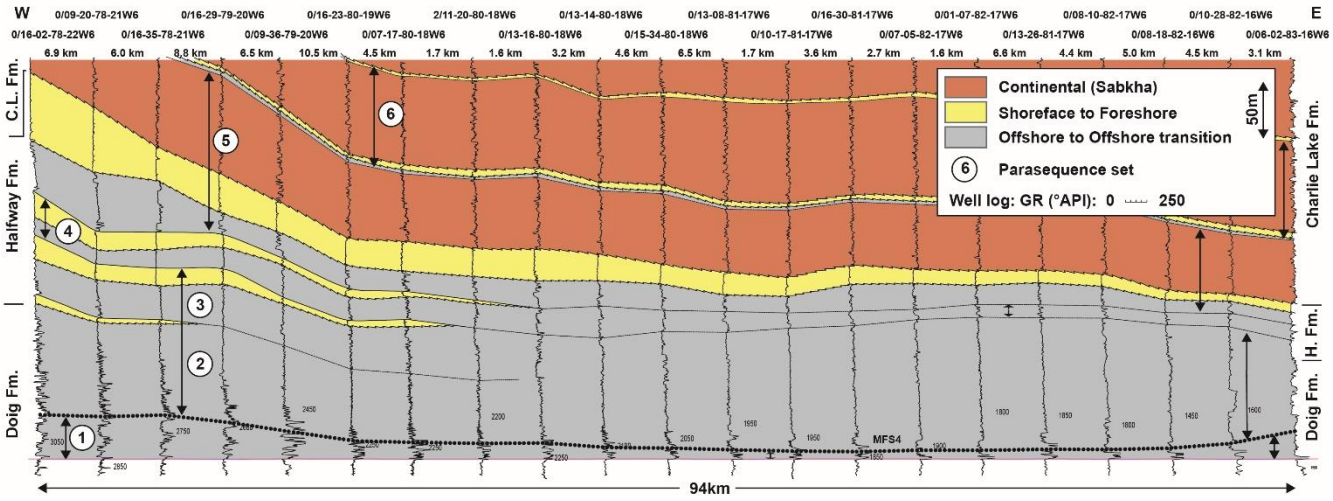
W
E
0/09-20-78-21W6
0/16-29-79-20W6
0/16-23-80-19W6
2/11-20-80-18W6
0/13-14-80-18W6
0/13-08-81-17W6
0/16-30-81-17W6
0/01-07-82-17W6
0/08-10-82-17W6
0/10-28-82-16W6
0/16-02-78-22W6
0/16-35-78-21W6
0/09-36-79-20W6
0/07-17-80-18W6
0/13-16-80-18W6
0/15-34-80-18W6
0/10-17-81-17W6
0/07-05-82-17W6
0/13-26-81-17W6
0/08-18-82-16W6
0/06-02-83-16W6
6.9 km
6.0 km
8.8 km
6.5 km
10.5 km
4.5 km
1.7 km
1.6 km
3.2 km
4.6 km
6.5 km
1.7 km
3.6 km
2.7 km
1.6 km
6.6 km
4.4 km
5.0 km
4.5 km
3.1 km
C.L. Fm.
Halfway Fm.
Doig Fm.
Charlie Lake Fm.
H. Fm.
Doig Fm.
Continental (Sabkha)
Shoreface to Foreshore
Offshore to Offshore transition
Parasequence set
Well log: GR (°API): 0 250
50m
MFS4
94km

Figure 7

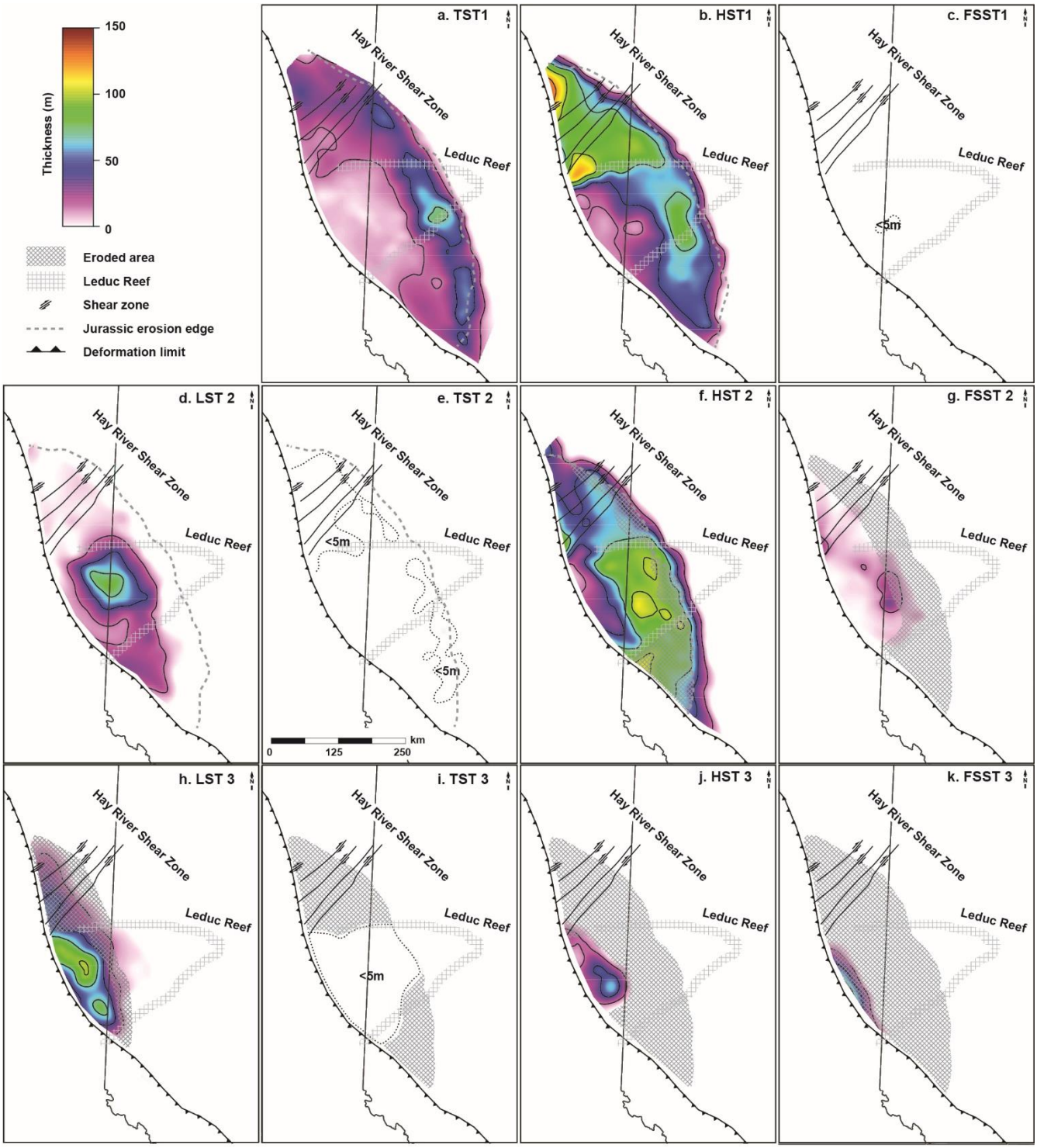
Thickness (m)
150
100
50
0
Eroded area
Leduc Reef
Shear zone
Jurassic erosion edge
Deformation limit
a. TST1
b. HST1
c. FSST1
d. LST 2
e. TST 2
f. HST 2
g. FSST 2
h. LST 3
i. TST 3
j. HST 3
k. FSST 3
Hay River Shear Zone
Leduc Reef
<5m
0
125
250
km

Figure 8

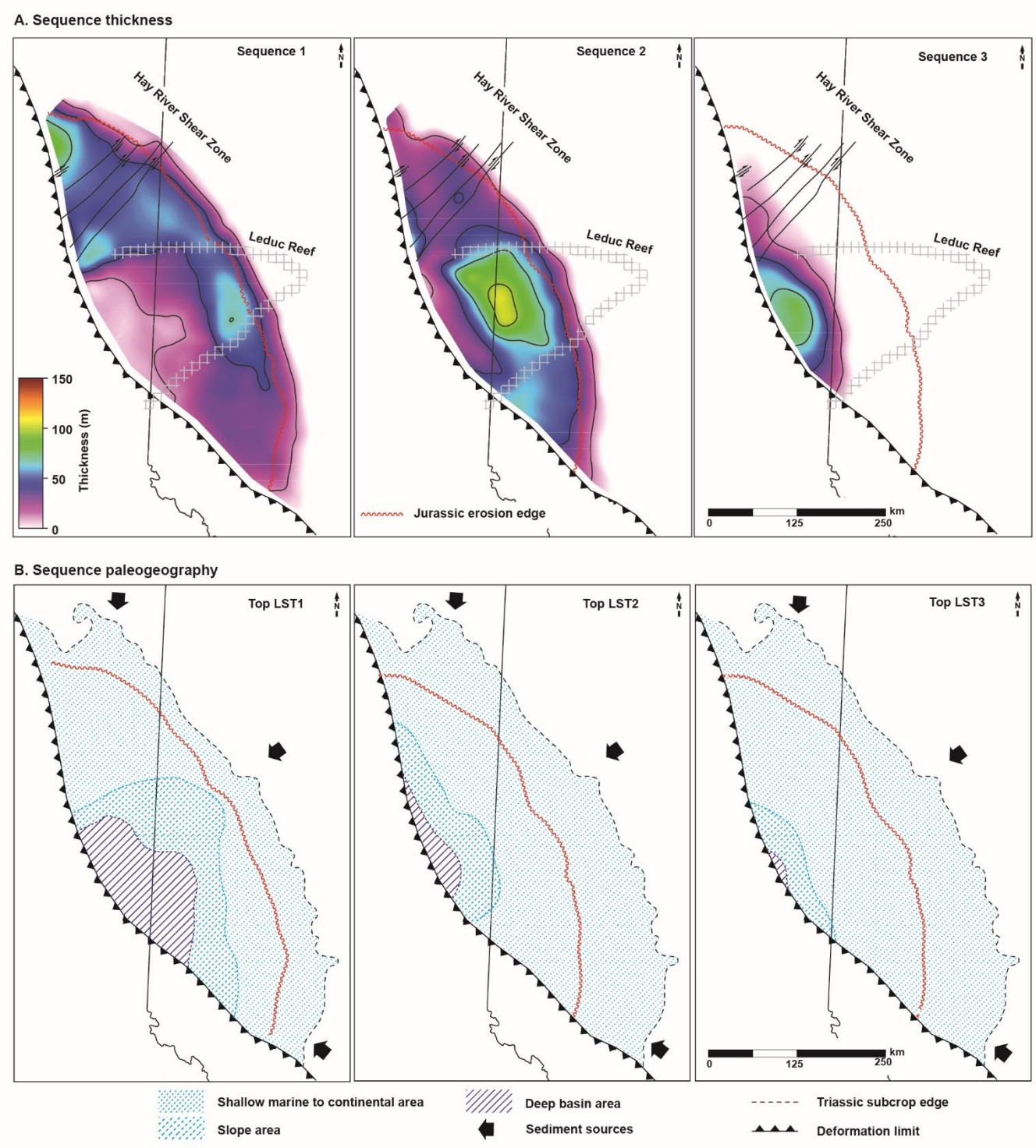
A. Sequence thickness
Sequence 1
Sequence 2
Sequence 3
Hay River Shear Zone
Leduc Reef
150
100
50
0
Thickness (m)
Jurassic erosion edge
km
0
125
250
B. Sequence paleogeography
Top LST1
Top LST2
Top LST3
Shallow marine to continental area
Slope area
Deep basin area
Sediment sources
Triassic subcrop edge
Deformation limit

Figure 9

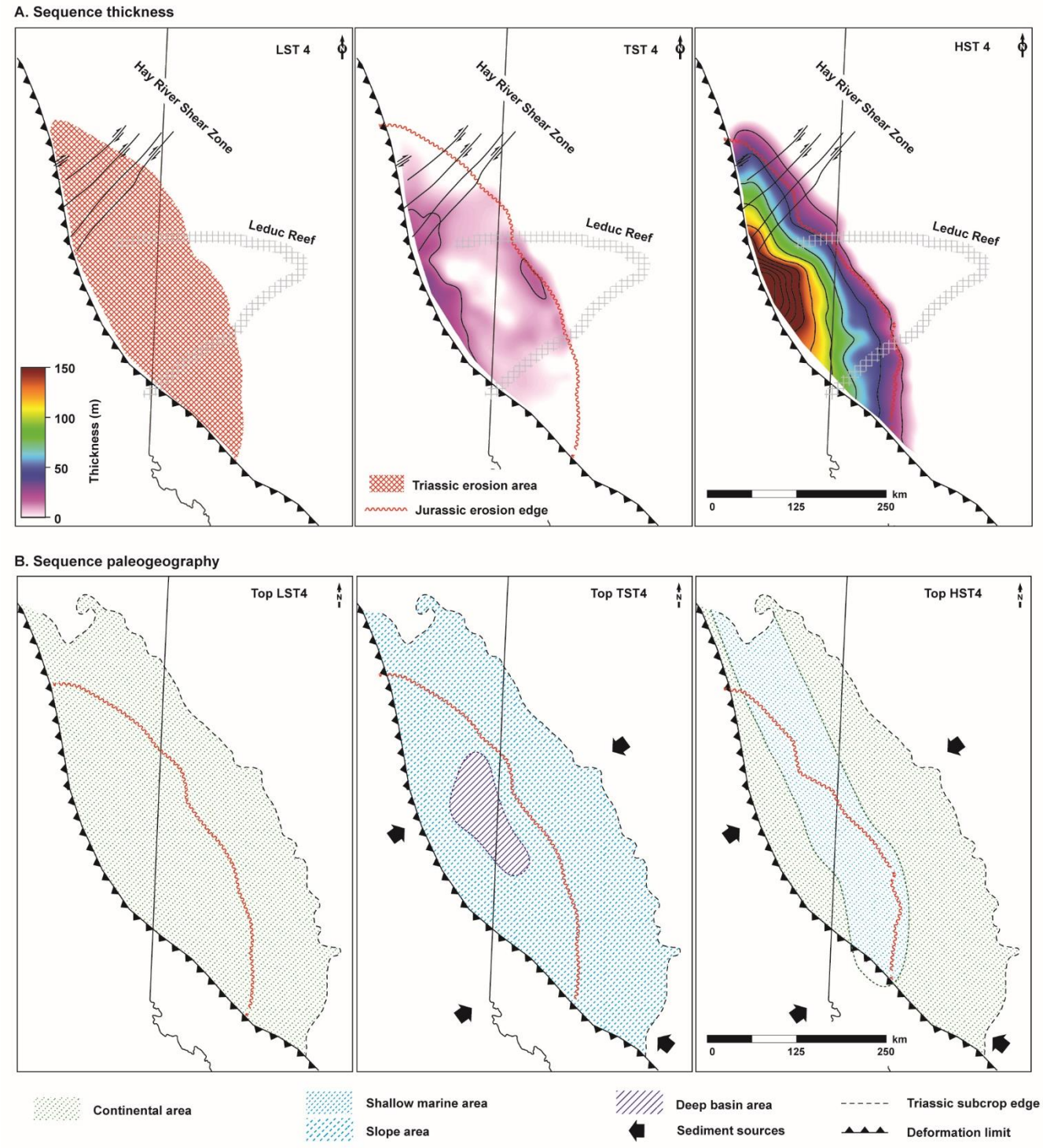
A. Sequence thickness
LST 4
TST 4
HST 4
Hay River Shear Zone
Leduc Reef
150
100
50
0
Thickness (m)
Triassic erosion area
Jurassic erosion edge
km
0
125
250
B. Sequence paleogeography
Top LST4
Top TST4
Top HST4
Continental area
Shallow marine area
Slope area
Deep basin area
Sediment sources
Triassic subcrop edge
Deformation limit

Figure 10

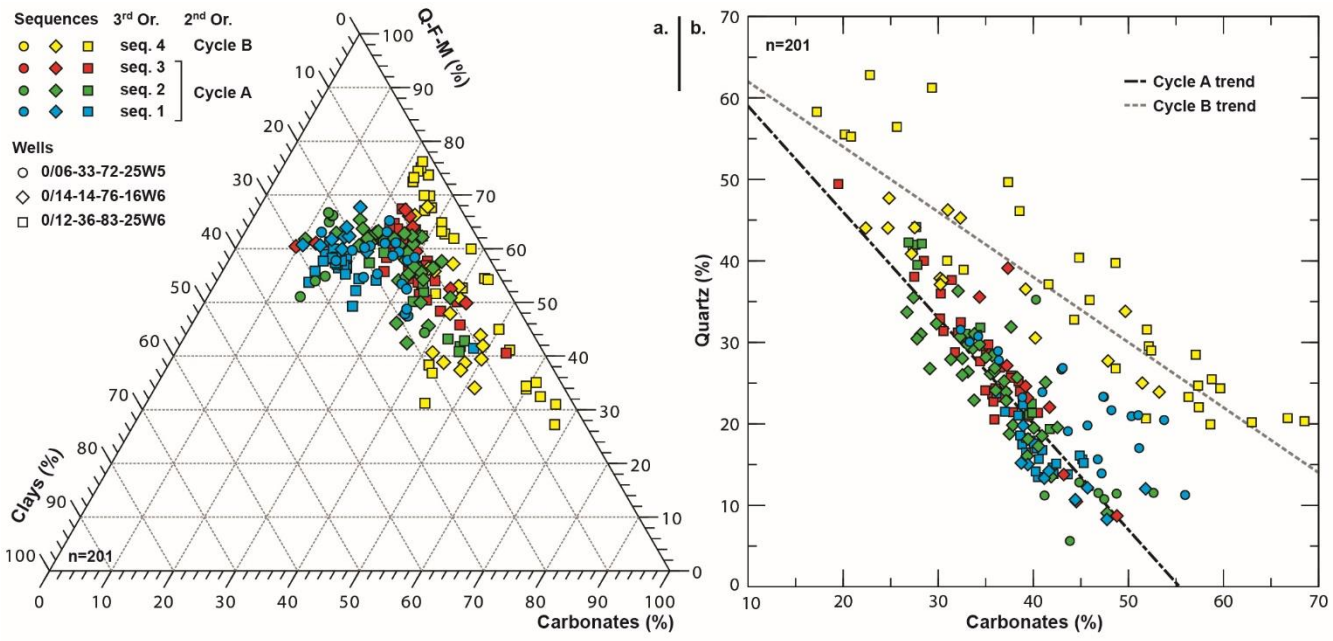
Sequences
3rd Or.
2nd Or.
seq. 4
seq. 3
seq. 2
seq. 1
Cycle B
Cycle A
Wells
0/06-33-72-25W5
0/14-14-76-16W6
0/12-36-83-25W6
n=201
Q-F-M (%)
Clays (%)
Carbonates (%)
a.
b.
n=201
Cycle A trend
Cycle B trend
Quartz (%)
Carbonates (%)

Figure 11

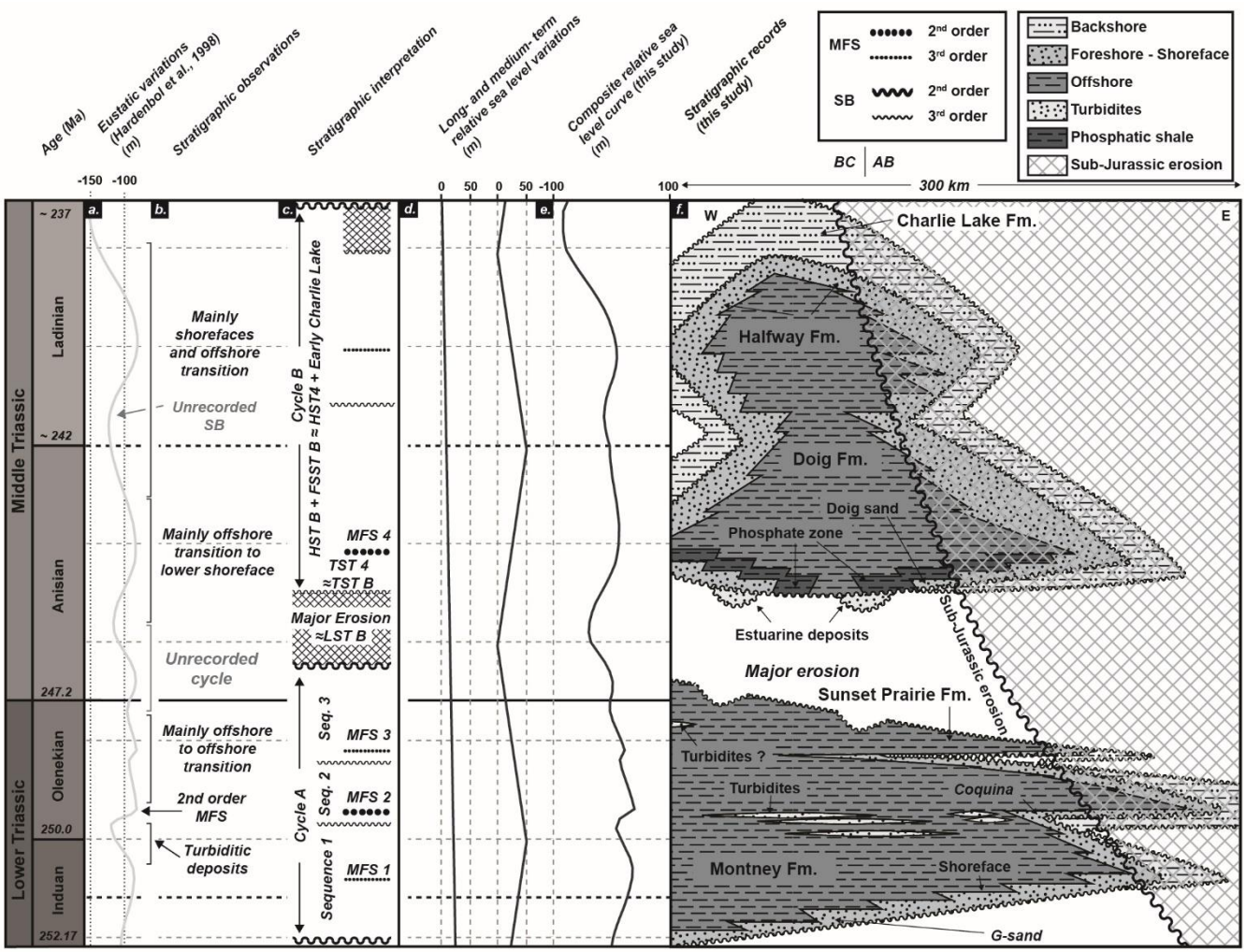
Age (Ma)
Eustatic variations (Hardenbol et al., 1998) (m)
Stratigraphic observations
Stratigraphic interpretation
Long- and medium- term relative sea level variations (m)
Composite relative sea level curve (this study) (m)
Stratigraphic records (this study)
MFS
2nd order
3rd order
SB
2nd order
3rd order
BC
AB
Backshore
Foreshore - Shoreface
Offshore
Turbidites
Phosphatic shale
Sub-Jurassic erosion
-150 -100
0 50 0 50 -100 100
300 km
Middle Triassic
Lower Triassic
Ladinian
Anisian
Olenekian
Induan
~ 237
~ 242
247.2
250.0
252.17
a.
b.
c.
d.
e.
f.
W
E
Mainly shorefaces and offshore transition
Unrecorded SB
Mainly offshore transition to lower shoreface
Unrecorded cycle
Mainly offshore to offshore transition
2nd order MFS
Turbiditic deposits
Cycle B
HST B + FSST B ≈ HST4 + Early Charlie Lake
MFS 4
TST 4
≈TST B
Major Erosion
≈LST B
Cycle A
Seq. 3
MFS 3
Seq. 2
MFS 2
Sequence 1
MFS 1
Charlie Lake Fm.
Halfway Fm.
Doig Fm.
Doig sand
Phosphate zone
Estuarine deposits
Sub-Jurassic erosion
Major erosion
Sunset Prairie Fm.
Turbidites ?
Turbidites
Coquina
Montney Fm.
Shoreface
G-sand

Figure 12